

# Practical implementation of Online Condition Monitoring of Lithium Ion Batteries using Pseudo Random Signals

---



Prepared by:

**Nigel Marowa**  
**MRWNIG002**

Department of Electrical Engineering  
University of Cape Town

Prepared for:

**Professor Paul Barendse**

Department of Electrical Engineering  
University of Cape Town

**November 2022**

Submitted to the Department of Electrical Engineering at the University of Cape Town in partial fulfilment of the academic requirements for a Bachelor of Science degree in Mechatronics Engineering.

**Key Words:** lithium-ion battery; state of charge; State of Health; AC impedance; PRBS; EIS; EEC, OCV

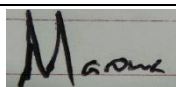
# Declaration

---

1. I know that plagiarism is wrong. Plagiarism is to use another's work and pretend that it is one's own.
2. I have used the IEEE convention for citation and referencing. Each contribution to, and quotation in, this final year project report from the work(s) of other people, has been attributed and has been cited and referenced.
3. This final year project report is my own work.
4. I have not allowed, and will not allow anyone to copy my work with the intention of passing it off as their own work or part thereof

**Name:** Nigel Marowa

**Signature:**



**Date:** 06 November 2022

# Terms of Reference

---

The topic for my undergraduate thesis, "Practical implementation of Online Condition Monitoring of Lithium-Ion Batteries using Pseudo Random Signals," was assigned to me by my advisor, Prof. Paul Barendse, in July 2022.

The following were the precise instructions provided by Prof. Paul Barendse:

1. Conduct a comprehensive analysis of the literature on Lithium-ion batteries, modelling strategies, performance evaluation, and state of health assessment.
2. Construct a battery equivalent electrical circuit model.
3. Construct a converter utilizing an electronic load to inject pseudo-random signals into the battery.
4. Review the findings and analyse the data.
5. Come to conclusions and offer suggestions

# Acknowledgements

---

Aside from my efforts, a lot of other people's encouragement and direction are crucial to the project's success. I would want to take this opportunity to thank everyone who contributed to the successful completion of this project. I couldn't have gotten this far without you.

First and foremost, I want to express my gratitude to God for providing me life and courage throughout the course of this undertaking. I would never have gotten this far without him keeping an eye on me.

I want to express my sincerest gratitude to my supervisor, Professor Paul Barendse, for lending this project the weight of his vast experience and expertise. His high standards have made me better today. I thank you for helping me finish this project.

To Mason, I am extremely grateful for your assistance and suggestions in the laboratory.

To all my friends who supported me throughout this journey. Bertha Mafunu, Peter, Tatenda and Ndangariro. I could never thank you guys enough.

Finally, In honour of my loving parents and siblings. I appreciate you giving me the tools and encouragement I needed to finish this assignment. I appreciate all the prayers, disciplining, patience and counsel you have offered me throughout the years. Without you, I could never have progressed this far, and I thank you.

# Abstract

---

Online battery impedance measurements offer insightful data on the charge and health of the battery, which can be used to enhance the related system's performance and safety. Despite being frequently used to measure battery impedance, electrochemical-impedance-spectroscopy (EIS) is not the best method for online measurements due to its complexity and slowness. Broadband signals, such as pseudo-random binary sequences (PRBS), which are quick and simple to use, can be used to overcome these shortcomings. The choice of the PRBS signal and the impedance measurements are both significantly impacted by the non-linear behaviour of batteries. The majority of PRBS signals can be used to measure linear systems, however signals for identifying non-linear systems are also available. The Literature Review of the battery is reviewed 1<sup>st</sup> in this paper. This is then accompanied by simulations in MATLAB/Simulink, showing the EIS and PRBS techniques using an electrical equivalent circuit. The setup is then implemented practically. The design and implementation of a bi-directional boost converter is a major part of this project. Its purpose being to inject perturbation signals in the battery cell and measure the voltage and current outputs to determine its impedance.

# Table of Contents

---

<b>1. Introduction.....</b>	<b>3</b>
1.1 Background to the study .....	3
1.2 Objectives of this study.....	4
1.2.1 Problems to be investigated .....	4
1.2.2 Purpose of the study .....	5
1.3 Scope and Limitations.....	5
1.4 Plan of development.....	5
<b>2. Literature Review .....</b>	<b>6</b>
2.1 Batteries (Basic Theory) .....	7
2.2 Models of Batteries.....	10
2.3 Battery Testing Techniques.....	13
2.3.1 Open Circuit Voltage SOC estimation Method .....	13
2.3.2 Static Capacity Test.....	14
2.3.3 Electrochemical Impedance Spectroscopy (EIS).....	14
2.3.4 Pseudo-random Sequences .....	15
<b>3. Methodology .....</b>	<b>19</b>
3.1 Simulation of Battery Model.....	19
3.2 Perturbation Signal (EIS and PRBS) in Simulink .....	22
3.2.1 EIS .....	23
3.2.2 Pseudo Random Binary Signals.....	25
3.3 Battery Monitoring Using Impedance Spectroscopy.....	27
3.4 Design Of Perturbation Signal And DC-DC Boost Converter .....	28
<b>4. Experimental Set Up.....</b>	<b>35</b>
4.1 Building the DC-DC Converter .....	35
4.2 PRBS Signal Generation and Sinusoidal Generation.....	38
4.3 Current and Voltage Measurements .....	42
4.3.1 Measurement of Inductor Current.....	42
4.3.2 Voltage Measurement.....	42
4.3.3 Implementation of the Bi-Directional Converter Overall .....	42
4.4 EIS and PRBS on Switching converter .....	44
<b>5. Results.....</b>	<b>46</b>
5.1 Battery Impedance Measurements.....	46
5.1.1 Plots During Discharge.....	46
5.1.2 Plots During Charging .....	47
5.2 Noise In Output and Inductor Current.....	48
<b>6. Discussion .....</b>	<b>49</b>
<b>7. Conclusions .....</b>	<b>50</b>
<b>8. Recommendations .....</b>	<b>51</b>
<b>9. List of References .....</b>	<b>52</b>
<b>10. Appendices .....</b>	<b>54</b>
<b>11. EBE Faculty: Assessment of Ethics in Research Projects .....</b>	<b>57</b>

## List of Figures

Figure 1.1: Internal Resistance of a battery [1] [2] .....	3
Figure 2.1: The Nyquist plot .....	6
Figure 2.2: The Discharging and Charging Process of the Lithium-ion Battery [5] .....	8
Figure 2.3: Description of individual cell components with equivalent circuit elements .....	9
Figure 2.4: The Resistive Thevenin battery model .....	11
Figure 2.5: Thevenin battery model with one RC .....	11
Figure 2.6: Thevenin battery model with two RC's .....	12
Figure 2.7: The structure of a multilayer feed-forward neural network. ....	12
Figure 2.8: The Static Capacitor Test [11] .....	14
Figure 2.9: Simplified linear Representation of an EIS measurement with a sinusoidal current injection and voltage response .....	15
Figure 2.10: Nyquist Plot of a Lithium-Ion cell .....	16
Figure 2.11: Nyquist Plot of a Lithium Iron Phosphate Cell .....	16
Figure 2.12: A Single PRBS signal period (one pseudo-random binary sequence) .....	17
Figure 2.13: A Typical PRBS signal power spectrum. The form adheres to a sinc function envelope. [18] .....	18
Figure 3.1: [22] Nyquist plot of impedance results obtained from V. Ovejas and A. Cuadras .....	19
Figure 3.2: [22] Nyquist plot of impedance results obtained from V. Ovejas and A. Cuadras .....	20
Figure 3.3: Nyquist plot of impedance results obtained from S. Moore [18]. ....	20
Figure 3.4: Nyquist curve .....	20
Figure 3.5: Battery Electrical Model .....	21
Figure 3.6: The Full electrically equivalent model of the fictitious cell in Simulink .....	21
Figure 3.7: 10 Pieces of 3.7 V Volt Rechargeable US18650 VTC5 .....	22
Figure 3.8: A Straightforward variable resistor to regulate signal disturbances flowing through the cell in the Simulink's environment .....	23
Figure 3.9: The Simulink Circuit used to run EIS Experiments .....	23
Figure 3.10: The EIS Signal fed into the Circuit shown in [3.9] .....	24
Figure 3.11: The Simulink Circuit used to run PRBS Experiments .....	25
Figure 3.12: Power Spectrum of PRBS Signal over a range of frequencies .....	26
Figure 3.13: The PRBS Signal fed into the Circuit shown in [3.9] .....	26
Figure 3.14: Operation of EIS on a Switching Converter .....	28
Figure 3.15: System Model .....	28
Figure 3.16: The Bi-directional Boost Converter .....	29
Figure 3.17: Switch 1 ON and Switch 2 OFF on the Boost Converter .....	30
Figure 3.18: Switch 1 OFF and Switch 2 ON the Boost Converter .....	31
Figure 3.19: Voltage and current waveforms for the capacitor and inductor respectively .....	31
Figure 3.20: Drive Circuitry System .....	34
Figure 4.1: Bi-directional Boost converter .....	36
Figure 4.2: LAUNCHXL-F28379D Launchpad .....	36
Figure 4.3: Block Parameter for PWM Generation .....	37
Figure 4.4: LAUNCHXL-F28379D Output ports .....	37
Figure 4.5: Interface between Simulink and LAUNCHXL-F28379D Launchpad .....	38
Figure 4.6: PRBS generation in Simulink .....	39
Figure 4.7: PRBS Generation using a 9-bit circuit .....	39
Figure 4.8: PRBS Signal Output .....	39
Figure 4.9: 3320A 20 Mega Hz function generator .....	40
Figure 4.10: Sinusoidal Perturbation from Function generator .....	41

Figure 4.11: Mosfet Driver with two Transistors .....	41
Figure 4.12: Boost Converter .....	42
Figure 4.13: Front view of the boost converter .....	43
Figure 4.14: Mosfet Driver and F28379D Launchpad.....	43
Figure 4.15: Li (NCoMn)O <sub>2</sub> Cell.....	43
Figure 4.16: Experimental Set of the battery and circuit breaker .....	44
Figure 4.17: Experimental Set Up for EIS and PRBS Measurements .....	44
Figure 4.18: Simplified model of the system.....	45
Figure 4.19: FFT Operation .....	45
Figure 5.1: Results on a switching converter at 100% SOC whilst Discharging .....	46
Figure 5.2: EIS(Yellow)and PRBS(Orange) at 100% SOC whilst Discharging.....	46
Figure 5.3: EIS(Yellow)and PRBS(Orange) at 100% SOC whilst Charging.....	47
Figure 5.4: Results on a switching converter at 100% SOC whilst Charging .....	47
Figure 5.5: Output Current through the load.....	48



# 1. Introduction

---

## 1.1 Background to the study

For large-scale, heavy current applications, lithium-ion batteries are swiftly overtaking other energy storage options in terms of popularity. Not only due to their rising energy density but also due to the sharp decline in production costs over the previous ten years. Lithium-ion batteries are revolutionizing the field of environmentally friendly engineering, from electric vehicles to the storage of renewable energy on the grid.

These intriguing new possibilities, however, also carry with them a host of issues that need immediate attention. Most people, and with good reason, immediately think of the danger that lithium entails. Lithium is a highly reactive material when it is an element. And the dangers of exploding or catching fire have been severe when enclosed securely in a foil shell (i.e., a cell). Also, one of the primary things holding back development is still the price of batteries. Therefore, discovering strategies to lengthen the life of pricey batteries is essential for future endeavours. Finally, a battery cannot be expected to operate at its maximal capacity on a continuous basis because the chemical reactions occurring inside a cell heavily depend on the surrounding environmental factors. Each of these difficulties emphasizes the requirement for precise, integrated condition monitoring systems in batteries. Thus, the impetus behind this inquiry.

In academic literature, a variety of potential approaches have been put forth. A cell's internal impedance values across a range of frequencies are frequently extracted, and this is the common goal. Typically, a battery management system incorporates any existing "online" monitoring systems (BMS (Battery Managing System)). They monitor standard voltage and current measurements for drainage and/or charging as well as temperature readings from sensors placed close to the surface of each cell's shell. Such systems have problems because they rely on overly simple models. Simply said, monitoring and evaluation simply concern the DC (Direct Current) profile of the cell. Figure 1.1 depicts the simplified DC profile of a cell as represented by the electrically equivalent circuit (EEC). A model like this, however, neglects several elements that could assist reveal key facts about a battery. In three major areas, State of Health (SOH), State of Charge (SOC), and Remaining Useful Life (RUL) predictions, more complex modelling is essential.

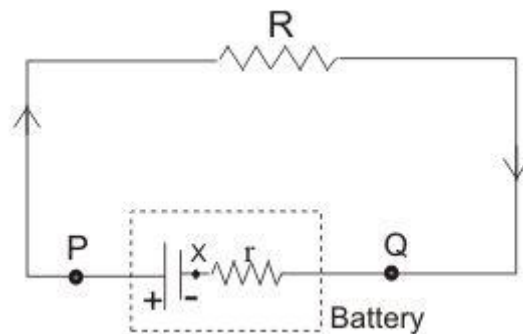


Figure 1.1: Internal Resistance of a battery [1] [2]

A more precise description of an electrochemical cell's AC impedance response includes both reactive behaviour and pure internal resistance. Electrochemical Impedance Spectroscopy is the first and most popular technique (EIS (Electrochemical Impedance Spectroscopy)). Its capacity to gauge a cell's resistance throughout a large frequency range is indicated by the term, which is general. All of the

more advanced strategies try to achieve this. They differ in the way that the frequency spectrum is recognized and transmitted. EIS employs a variety of unique sine wave disturbances (small variations in the current passing through the cell). Broadband Impedance Spectroscopy (BIS), on the other hand, combines a similar sweep of sine waves into a single multi-sine signal. Although BIS can be completed fast, there are issues related to the structure of high-resolution sinusoids.

The most recent development around complex impedance measurement is pseudo-random binary sequence (PRBS) injection techniques. Tests and experiments with PRBS will be the main topic of this study. The main goal is to produce a repeated series of fluctuating rectangular waves that together constitute a band-limited white noise spectrum, allowing for the isolation and identification of the cell's AC properties. It has been demonstrated to have accuracy levels that are comparable to those of industry-standard EIS techniques, making it perhaps the most promising method for fast, online impedance measurements. The hypothesis is still being developed; therefore, more thorough research is needed before it can completely realize its promise.

This report is both theory and practically based and we will see that it has the advantage of being able to explore a broad range of digital simulation-scenarios and real scenarios, which could give valuable information in the near future.

## **1.2 Objectives of this study**

### **1.2.1 Problems to be investigated**

The questions to be investigated are as follows:

#### **What are the most often used energy technologies in the world?**

Literature review will be done electrochemical cells

#### **How is PRBS used, and what details about a battery cell may it reveal?**

Literature review will be done electrochemical cells and the study of EIS and PRBS techniques

#### **What converter topologies are currently being applied to battery interfaces in industry?**

Create, model, and construct a switch mode converter that can connect to a battery.

#### **Can perturbation signals be accurately monitored using signal analysis techniques after being introduced into the Li-Ion cell?**

Design a Mosfet gate driver circuit as well as implementing a microcontroller to control the perturbation signal

### **1.2.2 Purpose of the study**

The research proposal is as follows:

“Practical implementation of Online Condition Monitoring of Lithium-Ion Batteries using Pseudo Random Signals.”

The purpose of the work/project

- Implementation and design of a bidirectional boost DC-DC converter to inject perturbations signal into a battery through a load for Impedance measurements. This would lead to the evaluation of the battery's state of charge, state of health and performance of the battery.

## **1.3 Scope and Limitations**

The goal of this study was to expand both the theoretical and practical knowledge base for methods of online impedance measurement. A variety of repeatable testing techniques were designed to fit with simulation settings. It's important to note that these were created to operate as closely as possible to real-world setups. Verification and further optimization of modern pseudorandom signal theory were the main objectives. Practically speaking, a boost converter was created to inject both Sinusoidal and PRBS signals. Broadband Impedance Spectroscopy is not examined in the same depth as PRBS, but instead is based on findings from related research projects. Instead, the contrast between the PRBS results and the EIS, the current industry standard, received a lot of focus.

## **1.4 Plan of development**

The 1st chapter of this report starts with the Literature review of the Lithium ion cells. This chapter is followed by the Methodology chapter. This is where the experimental process is explained in detail specifying and calculating all the parameters that are crucial in performing the EIS and PRBS experiments on the Lithium-ion cell. The design and parameterisation of the boost converter is also explained in the section. The use of the micro controller to produce PRBS signals is touched in this section as well as in chapter four. Chapter four focuses on the implementation of the methods deduced in chapter three, both in simulation and practical. Chapter five is when the results are analysed of the whole system. Comparison between EIS experiments and PRBS experiments is also done in this part of the report. Chapter six, seven and eight all focus on results obtained and how certain adjustments can be done to improve the entire experiment both at present and in the near future.

## 2. Literature Review

An overview of modern battery technology and the field of battery testing is provided in this chapter. Additionally, it reviews online Impedance Spectroscopy methods and literature-based EIS, BIS, and PRBS methods.

The need for extended battery life is highlighted by the growing use of lithium-ion batteries in daily life. In this context, battery endurance, or how long a pack or cell can operate without needing to be recharged, is referred to as battery life. While there are different ways to enhance battery life (more efficient parts or batteries with greater capacity), there is also a higher expectation for the state of charge (SOC) [3] prediction's accuracy in these applications. Additionally, for bigger battery systems, such as those found in electric vehicles, there is a desire for greater longevity and even second life applications. The monitoring of state of the battery's condition will be discussed below.

Electrochemical impedance spectroscopy (EIS) [4], broadband impedance spectroscopy (BIS), and pseudo-random sequence (PRS) injections are the three main methods used in the field of battery state monitoring. They are all aimed towards recording a cell's distinctive complicated impedance curve and determining the cell's health based on how the curve behaves over time.

EIS is a very precise technique for figuring out the SOC and SOH of battery systems [3] [5] [4]. The EIS approach was used initially in this research due to its superior accuracy when compared to alternative methods and the fact that it enables estimation of both the SOC and the SOH by a single test that includes an AC frequency sweep. The EIS method measures the cell's impedance through a variety of AC pulses of varied frequencies. Figure 1 shows an example of a Nyquist plot that can be used to depict the measured impedance. [6]

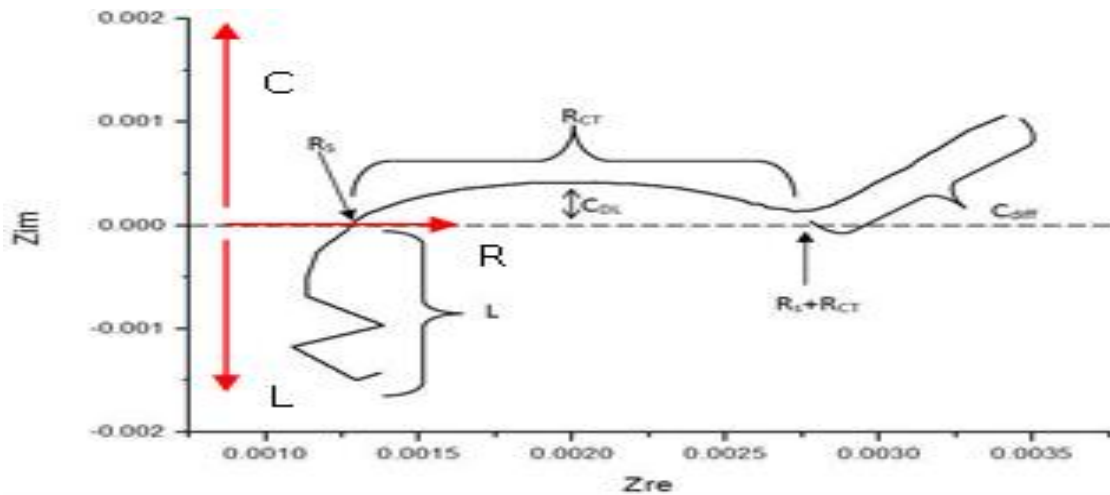


Figure 2.1: The Nyquist plot

The impedance result of an AC excitation voltage will be a complicated number since the electrochemical cell possesses both inductive and capacitive features. As a result, the current and voltage waveforms will be out of phase and provide both a phase angle and magnitude. Since the many components respond differently to each individual frequency, the wide frequency range of the AC signals given to the cell allows for the study of each individual component.

A measurement point on the X axis (real impedance) represents a fully resistive impedance since a pure resistance has no phase change. There is a capacitive component to the impedance, as seen by a measurement point above the X axis, with a phase shift angle ranging from -1 to -90 degrees. An impedance measurement point located below the X axis reveals the presence of an inductive component with a phase shift angle between 1 and 90 degrees. This is depicted in Figure 1, and the resistive, capacitive, and inductive qualities are further underlined by the red arrows.

BIS may be more appropriate for online monitoring since a single test can be completed quickly enough to eliminate the impacts of the cell's shifting state of charge (SOC). However, compounding numerous sine waves in a single perturbation, has additional complications: Signals can quickly become excessively big, pushing the battery beyond its linear zone. Pseudo-Random Signals, whether in binary or ternary form, offer a workable substitute while preserving a level of precision suitable for the majority of online applications.

This document is an extension of a 2020 project in which the system was modelled. The system's implementation will be the main emphasis of this project. The underlying knowledge required to lay the groundwork for the experimentation method in science is covered in the sections below: I'll start with internal impedance, which is the main emphasis of battery modelling. The techniques for simulating an internal impedance model are then reviewed.

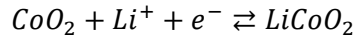
## 2.1 Batteries (Basic Theory)

A device that transforms chemical energy into electrical energy is an electrochemical cell. One or more of these cells are combined to form a battery. In this sense, a unitary cell is the simplest type of battery. The primary cell type (not rechargeable) and the secondary cell type of batteries were developed later over several centuries (rechargeable). The lithium-ion battery is a contemporary improvement over the lithium battery and, in contrast to lithium batteries, is rechargeable.

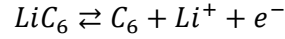
A battery is made up of an electrolyte, a separator, a positive electrode, and a negative electrode. Graphite is the most popular negative electrode material. Lithium cobalt oxide, lithium iron phosphate, or lithium manganese oxide are often the materials used to make the positive electrode. Lithium salts in ethylene carbonate generally make up the electrolyte. Lithium salts are frequently utilized, and some examples are lithium hexafluorophosphate ( $\text{LiPF}_6$ ) and lithium hexafluoro arsenate monohydrate ( $\text{LiAsF}_6 \cdot \text{H}_2\text{O}$ ) [7]. It consists of a thin, porous polymer sheet made of polyethylene or polypropylene.

The positive electrode (cathode) is typically made of  $\text{LiCoO}_2$ , and the negative electrode is made of graphite (C6) (anode). Lithium ions can enter and exit either electrode's structure during intercalation or deintercalation operations. During discharge, the electrons flow through the external circuit in the same direction as the positive lithium ions as they go from the negative electrode (often graphite) to the positive electrode (creating a lithium compound) through the electrolyte.

A current collector, which is typically constructed of aluminium, connects the positive terminal to the cathode. Lithium ions can be released by the cathode material during charging and absorbed during discharge. With the help of the electrons that go through the external circuit, these ions mix or separate, as appropriate. The reduction equation that follows, for instance, illustrates the chemical half-reaction that would occur during the discharge of a  $\text{LiCoO}_2$  cathode. [7] [8] [9] [6]



The half-reaction of the negative (anode) electrode:



Thus, the entire reaction can be expressed as:

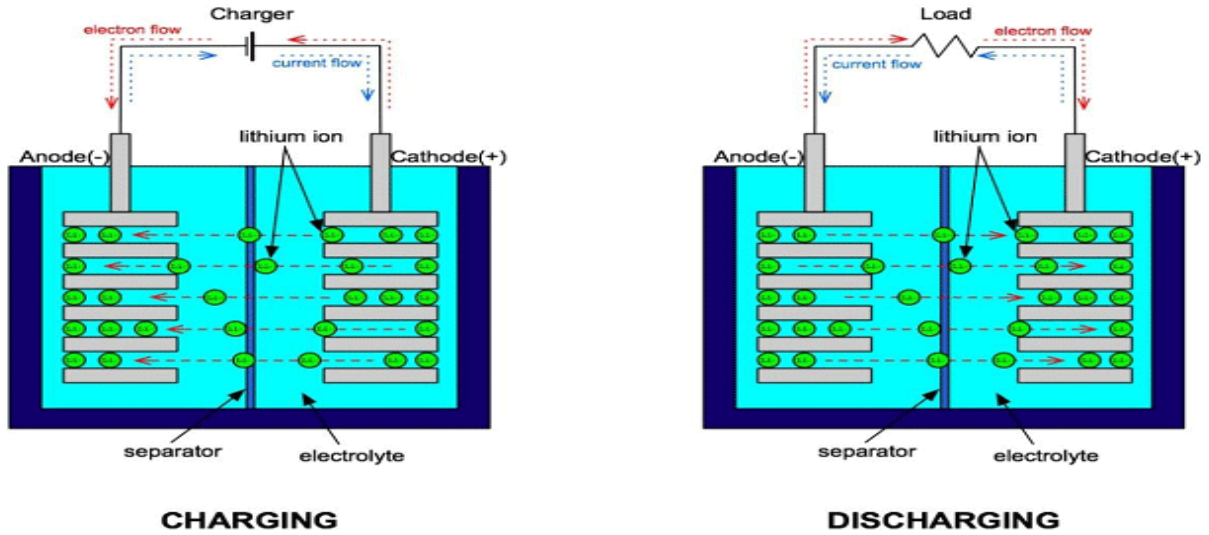
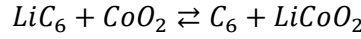


Figure 2.2: The Discharging and Charging Process of the Lithium-ion Battery [5]

One of the most important elements is the separator. The first function is that it acts as a safety mechanism, guarding against internal short-circuiting and excess potential. Second, the ability of the separator to stop electron flow while permitting lithium ions to move between the anode and cathode is necessary for the Redox reaction mentioned above. Many layers of polyethylene and polypropylene are typically combined. [5] [10] The edge of the anode intercalation material will accumulate a layer known as the Solid Electrolyte Interphase (SEI) layer during the course of a cell's lifetime. This is a clear illustration of observable battery deterioration. The impedance curve gains a resistive-capacitive component as a result.

[11]

## Batteries Internal Impedance

Distinct parts of a cell's internal structure make different contributions to the total impedance. The real and imaginary components are plotted over a range of frequencies to create the characteristic curve, which is used to visualize a cell's resistance. Either a Nyquist plane or Bode plots can be used to do this. A typical Nyquist impedance plot with labels for the relevant regions of interest is given in Figure 2.1 shown previously.

Using this method, a typical Nyquist plot is displayed in Figure 2.1. The Nyquist plot can be divided into three main categories: high frequencies are connected to an inductive effect brought on by the geometry of the cell and the porosity of the electrode plates; the intercept with the real axis corresponds for the total value of the **ohmic resistances**; and low frequency behaviour can be connected to the capacitive effects. Additionally, the semicircle end corresponds to **Li<sup>+</sup> cation diffusion** in the solid-state phase at low frequency ranges where the graph may appear to spike.

The other semicircle is dependent on the electrode potential and is represented by a double-layer capacitance and a charge-transfer resistance. This semicircle corresponds to the relaxation of charge carriers at the **solid-electrolyte interface** (SEI) [10] [12]. The **Warburg impedance** is the Nyquist plot's diagonal line with a positive slope that begins at low frequencies. This impedance is a result of the solid-state diffusion of  $\text{Li}^+$  in the bulk electrode material, which is a chemical process.

It is possible to understand the **Warburg impedance** component as the Cdiff-designated straight line on figure 2.1. Various electronic components can be used to approach the Nyquist plot depending on the frequency ranges on which they have a significant impact. An inductance can be used to represent high frequencies, while a pure resistive element is represented by a cross at zero on the imaginary axis.

The semicircle on the plot is then modelled using an RC-parallel branch. Last but not least, the response at low frequencies is impacted by the Warburg impedance. By adjusting these circuits, it is possible to convert the Nyquist plots' visual data into parameters that change over time as the degradation process becomes more obvious. By doing so, a correlation between parameter changes and the battery's SOH can be established.

Figure 2.2 illustrates a method for describing the separate electrical and electrochemical constituents that make up a battery cell. The whole model for a battery cell is produced by connecting the corresponding circuit components in series. [10]

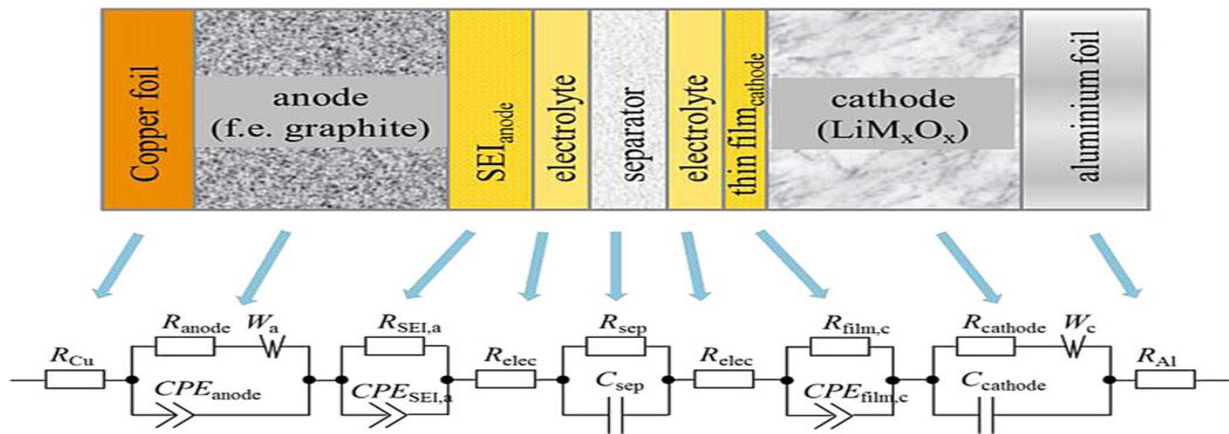


Figure 2.3: Description of individual cell components with equivalent circuit elements

## States of Batteries

Characterizing cells at a specific time point has been extensively studied. This may be due to inherent qualities like the operating/charging voltage resulting from the chemistry or operational state parameters like the battery's State of Charge and current output. Predicting its performance and operation requires knowledge of a wide range of information. A battery varies over time due to degradation and operating conditions, regardless of the information provided by the battery's manufacturer. It is crucial to understand how the battery's parameters will vary so that its performance may be optimized. This is not a simple task because a battery exhibits nonlinear behaviour as a result of intricate internal electrochemical reactions as well as adverse operating conditions.

The following list includes the most critical conditions to keep an eye on in order to ensure that the secondary battery continues to function.

- **State of Health (SOH) condition** is used to measure how much a battery has degraded over its lifespan and is directly connected to capacity. Both a battery's capacity and ability to transmit electricity decline as it ages. The relationship between SOH is given by the ratio of the current capacity to the capacity of the battery when it was new.
- **State of Charge (SOC)** in a battery at a given time is measured as a percentage. For instance, a computer's SOC reading could be % 70% full or 10% full. It is merely the proportion between a battery's capacity in a particular state and its overall capacity.

Since these states cannot be measured directly, they are estimated using other variables like voltage, current, impedance, and temperature. A suitable model for the electrochemical system must be defined in order to infer the states from the directly measurable parameters. This will be discussed in detail in the following section.

## 2.2 Models of Batteries

The battery modelling can be broadly divided into three groups. **Models for electrochemistry, mathematics, and electricity.**

**Mathematical battery models** are often analytical models made up of a large number of equations that describe the characteristics of the battery.

The internal **electrochemical operations** of the battery are described by electrochemical models using physics-based techniques.

The most accurate models are those based on differential equations. Due to the high computational cost of these 2 types of models, this thesis focuses on the usage of **electrical models**, also known as Equivalent Electrical Circuits (EEC) [12]. A passive electronic component model, also known as an EEC, is a sort of electrical model that is used to depict the battery states and estimate parameter values. Solving these models can be done using microcontrollers thus, enable accessibility of results in real time. EEC models are used to model parameters in order to maximize the model's complexity and accuracy.

Circuit components like resistors, voltage sources, capacitors, and inductors are used in EECs. Due to how simple they are to use; they have been widely used for EV battery technology.

### Simple battery model Rint model

The battery model that is most frequently used is shown in Figure 2.4. [12] It is made up of an ideal battery with an open circuit voltage (OCV), an internal resistance that is constant in value ( $R_{int}$ ), and a terminal voltage of  $v(t)$ . When fully charged, measuring the open circuit voltage can be used to estimate the terminal voltage  $v(t)$ , and adding a load and detecting both the terminal voltage and current can determine  $R_{int}$ . When a cell is fully charged, its SOC is 100%, and when it is totally drained, its SOC is 0%. The total capacity ( $Q$ ), expressed in Ah or mAh, is the amount of charge subtracted from 100-0%.

An entirely charged battery has a higher open circuit voltage than one that has just been depleted. Despite the  $R_{int}$  model's seeming simplicity, it ignores the internal resistance's changing nature as it relates to temperature, charge state, and electrolytic concentration.



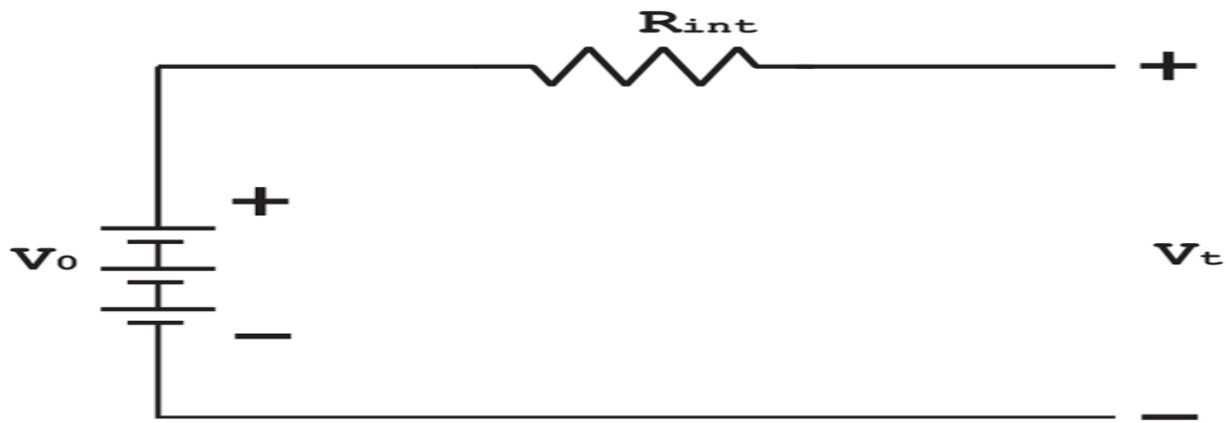


Figure 2.4: The Resistive Thevenin battery model

### Resistive Thevenin battery model

The resistive Thevenin battery model's circuit diagram is shown in Figure below. Internal resistances  $R_0$  and  $R_1$  of this model are tied to the battery's charging and discharging characteristics, respectively.  $R_0$  and  $R_1$ , which are internal resistances, model both electrical and non-electrical losses. Using one or more RC parallel branches, it is also possible to find diffusion voltages very closely. The model performs better than the  $R_{int}$  model, however it does not take into account transient phenomena like the capacitance effect. Due to its lack of dynamic behaviour, this model is inappropriate for use with electric vehicles and electric hybrids. Diffusion voltage, which can be roughly approximated using parallel RC branches, is the name for the slow reduction of voltage to zero that occurs in relaxation mode (Figure below1)

### An accurate mock-up of an electrical battery

Using a capacitor and a current-controlled source, An Accurate Electrical Battery Model simulates the battery's capacity, charging status, and run duration. The circuit accounts for both the sluggish and fast transient response as well as the battery life. It is possible to get over the barrier between SOC and open circuit voltage by using a voltage-controlled voltage source that is dependent on the state of charge (Figure 2.6).

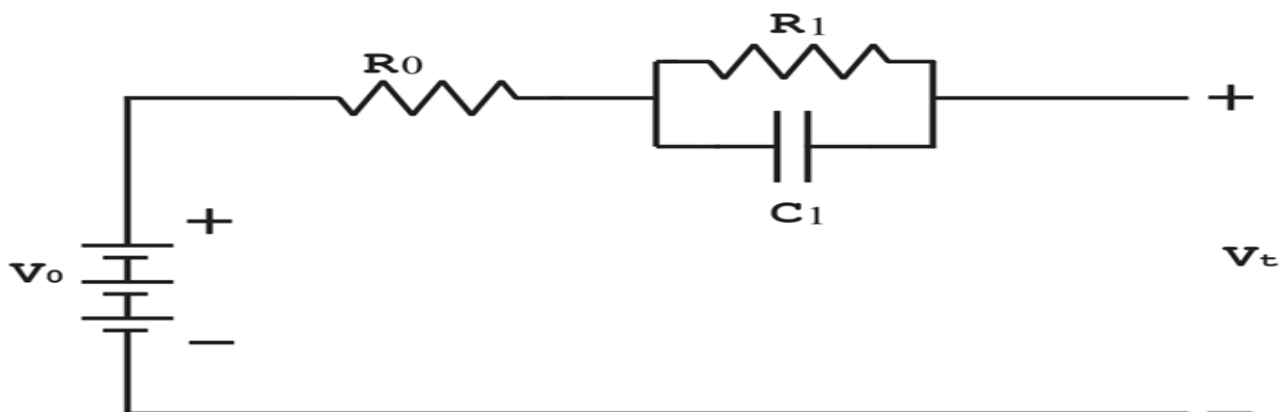


Figure 2.5: Thevenin battery model with one RC

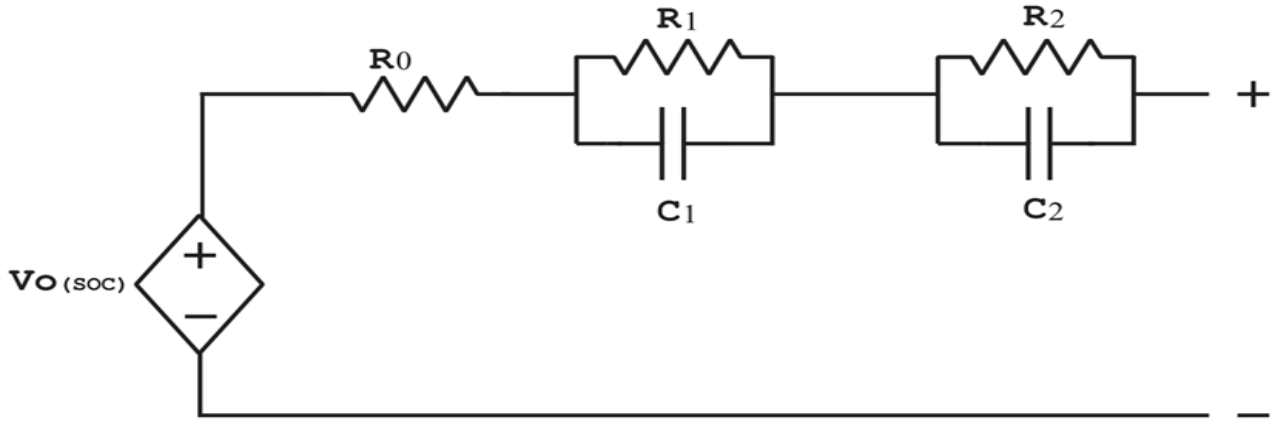


Figure 2.6: Thevenin battery model with two RC's

## Battery model using a neural network

A neural network is made up of three layers: an input layer with nodes to represent the input variables, one or more hidden layers with nodes to simulate the nonlinearity between the system input and output, and an output layer with nodes to represent the system output variable. The feed-forward neural network architecture for SOC estimation is shown in Figure below. The neural network's output, the battery SOC, is determined by the inputs of current (I), voltage (V), and temperature (T). Nodes connecting two neighbouring layers are linked together. The input layer does not perform any processing; it merely transmits the inputs with weights. The processing layers with the activation function at each node are the hidden layers and output layers.

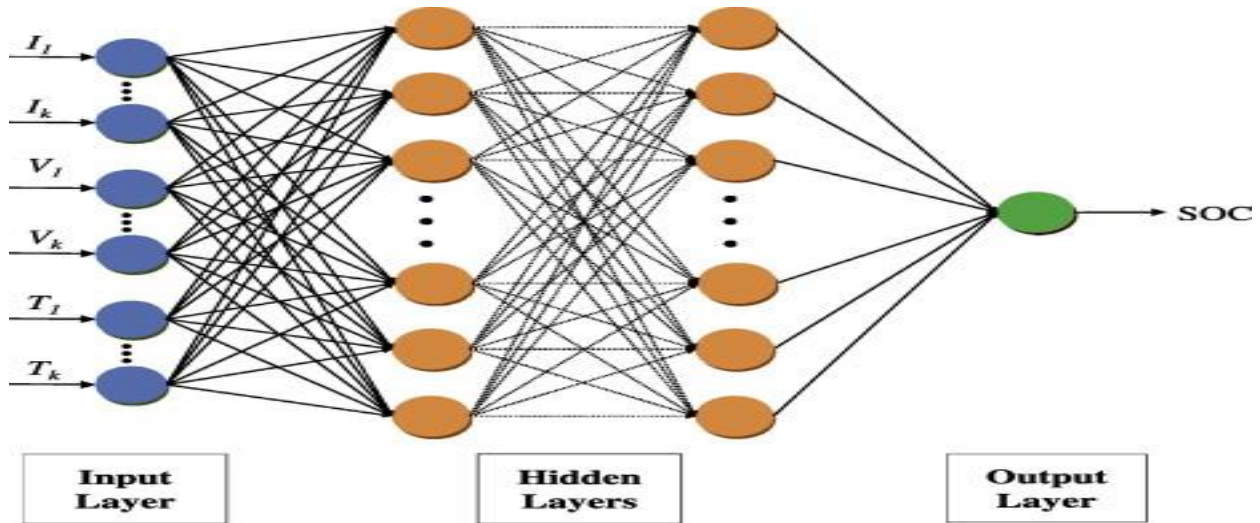


Figure 2.7: The structure of a multilayer feed-forward neural network.

## Electrical Battery Model

It is possible to create an electrically equivalent circuit (EEC) that mimics the cell's impedance properties. Each element of the chemical and physical make-up contributes an overall impedance that varies at various phases of charge, life cycles, and levels of health. In reality, after choosing an EEC model, a new cell's impedance shape can be parameterized by utilizing a best-fit version of the EEC impedance response [13]. The original parameterization can be compared to future readings as the cell ages to identify specific areas of degeneration or to simply estimate its state of charge/health.

The Levenberg-Marquardt Algorithm effectively combines the benefits of the steepest descent approach and Gauss-Newton for Complex Nonlinear Least Squares fitting of measured impedance data to an EEC model. It's crucial to remember that a model like this depends on the linear relationship between the battery's voltage, current and impedance, given by:

$$Z(j\omega) = \frac{V(j\omega)}{I(j\omega)}.$$

A Li-ion cell, which is fundamentally non-linear, must therefore be kept within operating zones that can be roughly described as linear during tests and simulations. More information on this will be provided in the approach section. However, in conclusion, there shouldn't be any substantial changes in the State of Charge (SOC), internal temperatures, or current throughput.

Computational effectiveness and exact match to the real electrochemical behaviour are the two main aspects that should be taken into account when selecting a model.

For a more accurate representation of the chemistry (and a plot that fits it better), additional circuit components (such parallel constant phase elements) can be added but doing so comes with a greater processing cost. In this study, a third-order Randle circuit is used as a "middle ground" representation to balance computational efficiency and accuracy.

## 2.3 Battery Testing Techniques

A number of battery testing methods are used to determine the battery states. This section looks into some of the most popular literary devices.

### 2.3.1 *Open Circuit Voltage SOC estimation Method*

Most applications require knowing how much more energy the battery system can give before a recharge is necessary, so knowing a battery's SOC is crucial. The SOC is comparable to a car's fuel gauge. It is a non-trivial task as batteries are nonlinear and have time-varying features, which make SOC not directly observable.

Inferring the SOC from the Open Circuit Voltage is a typical technique for determining the SoC of a battery system (OCV). The SoC can always be found by searching up the value of SOC for an OCV [14] if the relationship between the OCV curve and SoC is known. This is a straightforward method with great accuracy, but it has the significant drawback of requiring a lengthy period of battery rest before the OCV can be precisely measured [14]. It is only feasible to test after the system has been offline for a sizable period of time for an LFP cell at low temperature, as this can take up to 2 hours. For precise measurement, it has been advised in several texts that a settling time of at least 2 to 6 hours should be given [15]. The Electromotive Force (EMF) approach is used to resolve the problem with OCV estimate by tracking the relaxation time of the OCV method and forecasting the OCV by monitoring the voltage at any point in operation.

### 2.3.2 Static Capacity Test

An offline test called the static capacity test determines a cell's overall capacity. The process entails discharging the cell from a fully charged state until the voltage reaches a certain threshold. When LFP type cells were being charged and discharged, the static capacity test was conducted in [11]. The outcomes of a capacity test [11] conducted on an LFP type cell are shown in Figure below. This demonstrates the nonlinear relationship between capacity/SoC and cell voltage. The manufacturer specifies the maximum capacity of a cell, but due to operating factors like temperature and discharge rate, this value varies over time.

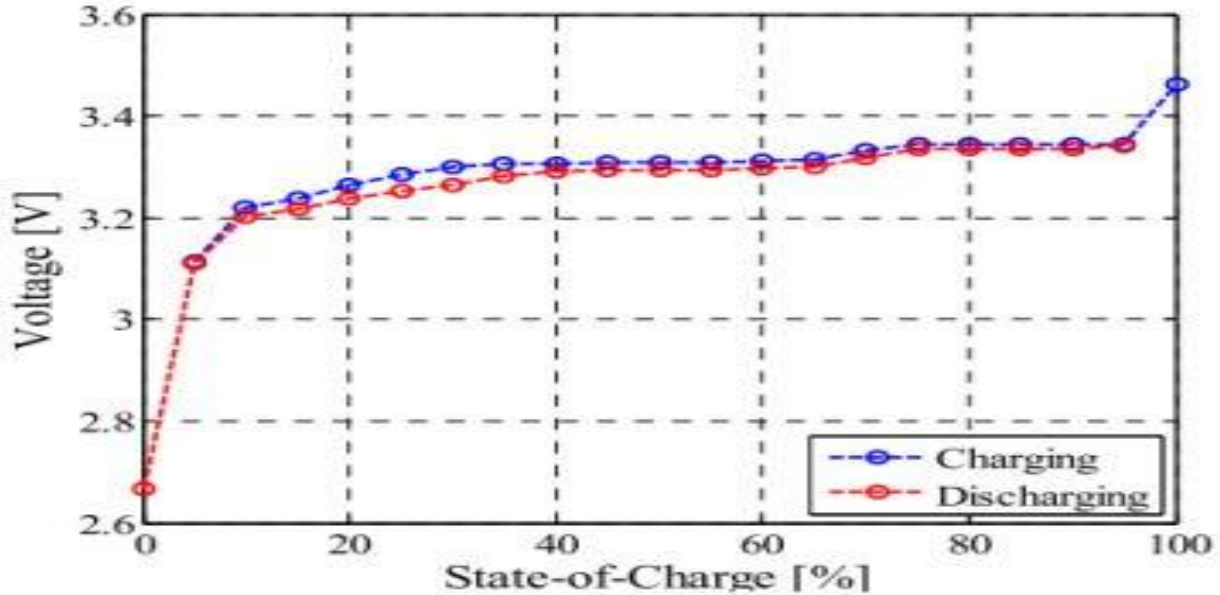


Figure 2.8: The Static Capacitor Test [11]

### 2.3.3 Electrochemical Impedance Spectroscopy (EIS)

The impedance of the battery can be determined using electrochemical impedance spectroscopy (EIS) at various frequencies. The battery manufacturer frequently specifies the impedance at 1 kHz; EIS builds on this by estimating impedance over a range of frequencies. EIS is a technique that involves applying a sinusoidal current or voltage to a cell and measuring the response, which is a sinusoid with amplitude and phase shift [16]. EIS approaches have been well studied in the literature, and it has been discovered that they are a valuable tool for determining the SOH, SOC, and SOF of electrochemical cells.

EIS is typically applied to electrochemical systems in one of two ways: Galvano-static mode or potentiostatic mode. Galvano-static mode involves injecting a current signal and measuring the voltage response. A voltage perturbation signal is employed in potentiostatic mode, and the current response is measured.

The Galvano-static mode is more frequently employed in electrochemical systems. The EIS measurement can be simplified to Figure below if we assume that a Li-Ion cell can be represented by a potential and an impedance  $Z_{battery}$ .

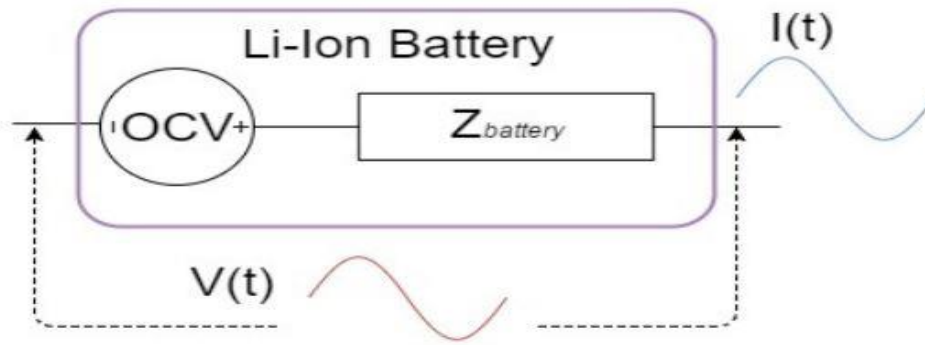


**Figure 2.9: Simplified linear Representation of an EIS measurement with a sinusoidal current injection and voltage response**

Between 20 mHz [17] and 10 kHz are the frequencies of interest [18]. This range is covered by the traditional "double semi-circle" impedance curve. To lessen the impacts of distorted noise, each frequency injection must cycle across a number of times, with the results being averaged. Another crucial component of the application of EIS is the perturbation signal's magnitude.

A signal that is too strong could disrupt the battery's intended initial DC operation in an online setting. In addition, the signal must not cause the battery to deviate from its linear Kramers-Kronig relations [17].

The Signal to Noise Ratio (SNR) of a signal that is too low, however, will not be enough [18]. According to the cell model under consideration, it is demonstrated in [19] that the optimal amplitude of a perturbation signal varies. A typical benchmark is 10% of the DC load current [18].

#### **2.3.4 Pseudo-random Sequences**

While generated via a deterministic technique, a pseudorandom binary sequence (PRBS), pseudorandom binary code, or pseudorandom bitstream is a binary sequence that is unpredictable and displays statistical behaviour comparable to a truly random sequence. In communications, PRBS generators are used for analogue-to-digital conversion as well as for time-of-flight spectroscopy, simulation, and encryption.

The main reason for using a pseudo-random sequence is that, theoretically, a whole test will be completed much more quickly than EIS processes. This decreases the consequences of high-discharge systems changing state during an impedance test, as was already mentioned. The two Figures below show how the impedance curves change as SOC drops.

The figures below are Nyquist diagrams showing how a cell's AC impedance characteristics alter with changing SOC

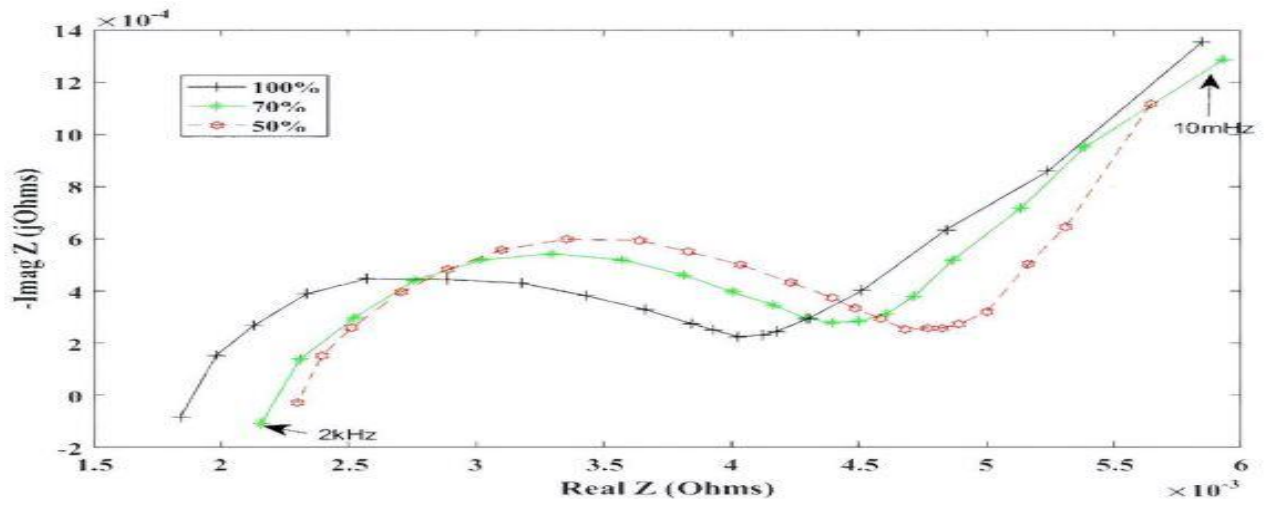


Figure 2.10: Nyquist Plot of a Lithium-Ion cell

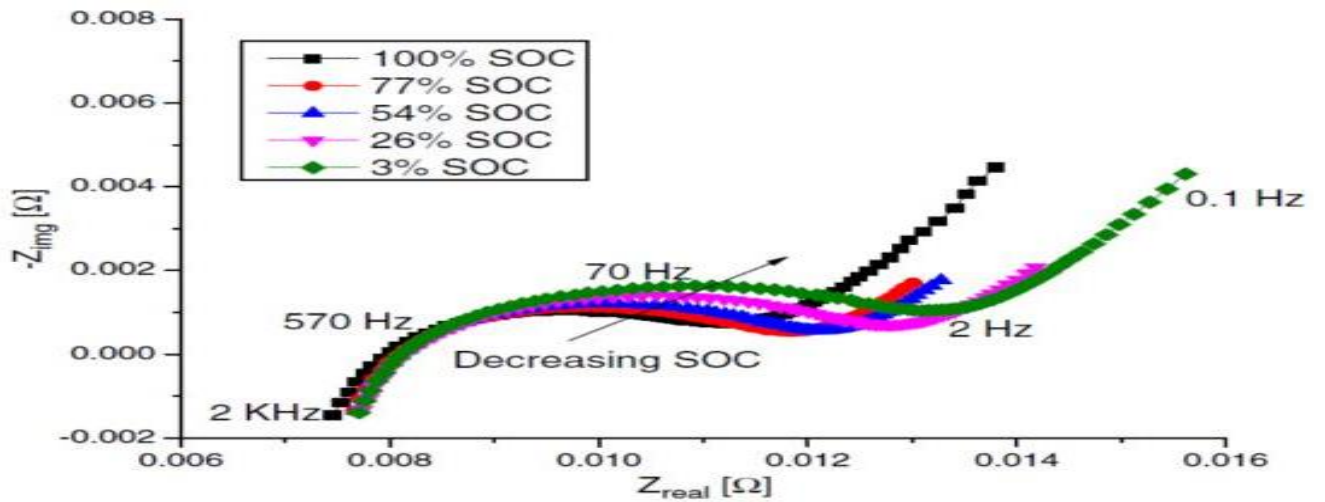
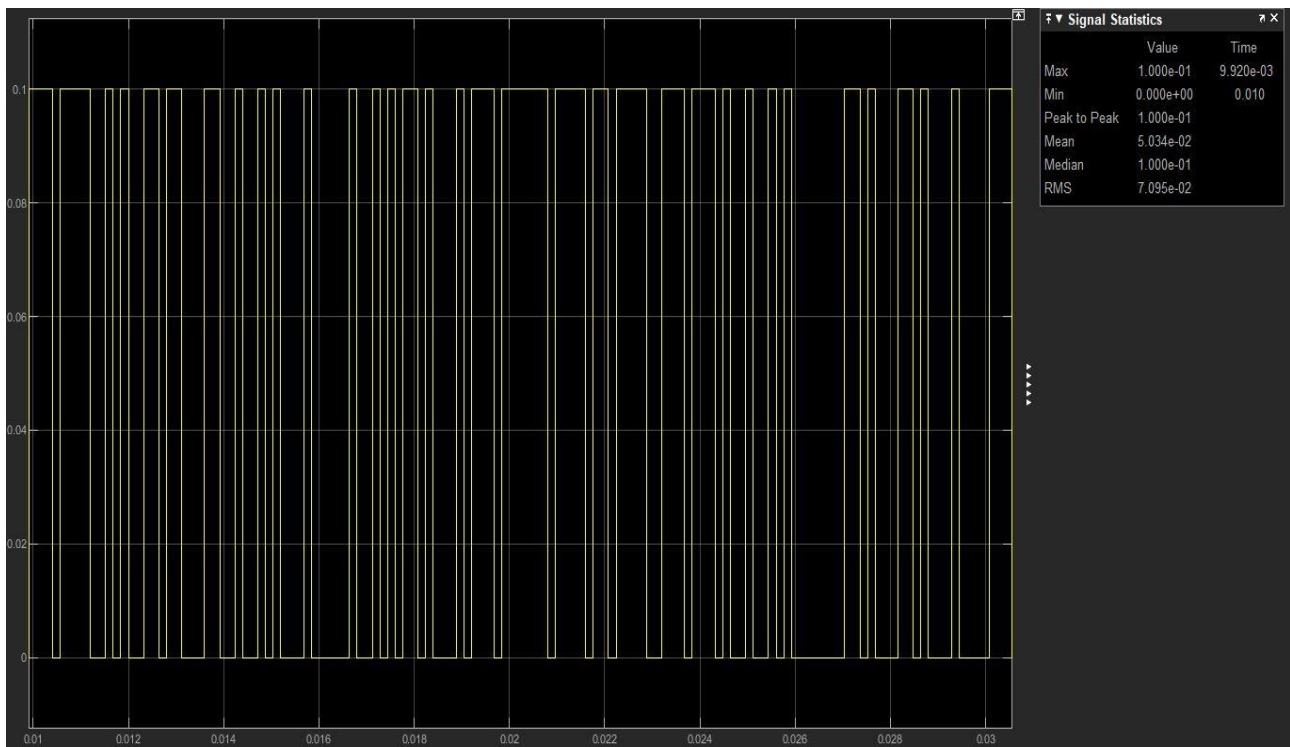


Figure 2.11: Nyquist Plot of a Lithium Iron Phosphate Cell

Kramers-linearity Kronig's conditions might be broken by a lengthy testing procedure like EIS that lasts long enough for a sizable decline in SOC to occur. To counter this, it has been demonstrated that PRS approaches only take about 10% as long as a comparable EIS procedure [20, 21].



**Figure 2.12: A Single PRBS signal period (one pseudo-random binary sequence)**

Figure above, displays a portion of a PRBS signal. Take note that there are 100 consecutive "randomly created" bits following the single period in this example.

The main characteristic of such a signal is that it has a frequency spectrum that resembles white noise over a controllable region. The lowest element of the spectrum is called  $f(\text{res})$ , or fundamental frequency.

A sinc-shaped power envelope is followed by components with increasing frequency, as seen Figure below.

Pay attention to how the power spectrum immediately crosses the zero-axis at  $f(\text{gen}) = 10\text{Hz}$ . At a third of  $f(\text{gen})$ , the -3dB point is reached (gen). A decreased signal-to-noise ratio (SNR) is produced at the output due to the abrupt drop in power at higher frequencies [20, 18]. This is clearly undesirable in a physical application when conflicting noise signals become a significant worry. As a result, the bandwidth of interest is selected as a somewhat uniform power band below  $f(\text{gen})$ . A. J. Fairweather, et al research.'s indicate that the maximum usable bandwidth must fall inside the -3dB window.

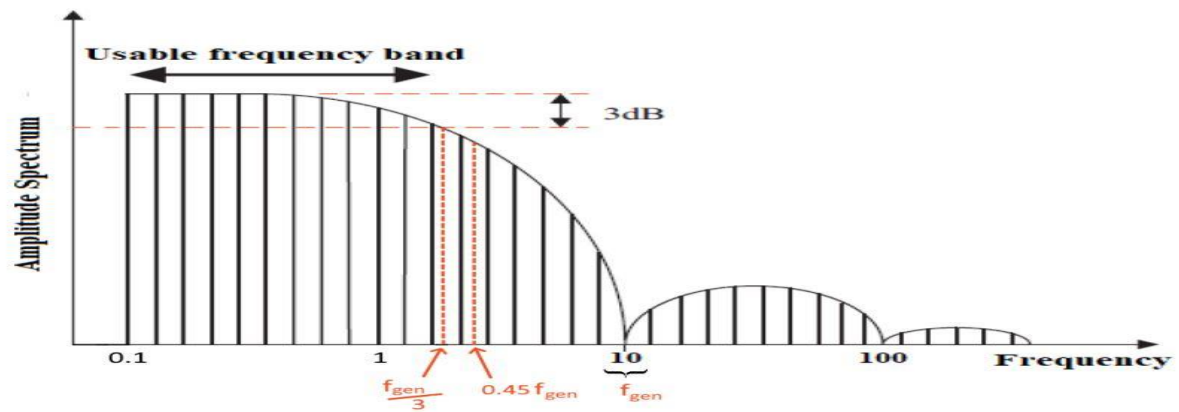


Figure 2.13: A Typical PRBS signal power spectrum. The form adheres to a sinc function envelope. [18]



### 3. Methodology

This section of the project will identify the exact methods or processes used to locate, choose, process, and evaluate data on the monitoring of batteries. More will be discussed in the following subsections.

#### 3.1 Simulation of Battery Model

##### Choice and Derivation of Parameters

A typical Li-ion cell was designed using the third order Randle model with a series inductance. According to a best-fit algorithm based on the Nyquist plots documented in [20] each passive component (resistor, capacitor, and inductor) in the model was configured. The model's overall impedance was derived mathematically, and theoretical charts were created using the following equation:

$$Z(j\omega) = j\omega L + R1 + \frac{1}{\left(j\omega C1 + \frac{1}{R2}\right)} + \frac{1}{\left(j\omega C2 + \frac{1}{R3}\right)} + \frac{1}{\left(j\omega C3 + \frac{1}{R4}\right)}$$

The series of images below display the Nyquist impedance plots that were used as guides while fitting a curve that resembled a true-to-life cell model. Due to its chemical composition, physical attributes, historical storage history, manufacturing method, and environmental factors, each cell will have a slightly distinct impedance curve. The goal of this inquiry was to combine information from many sources to produce a general plot based on the equation above.

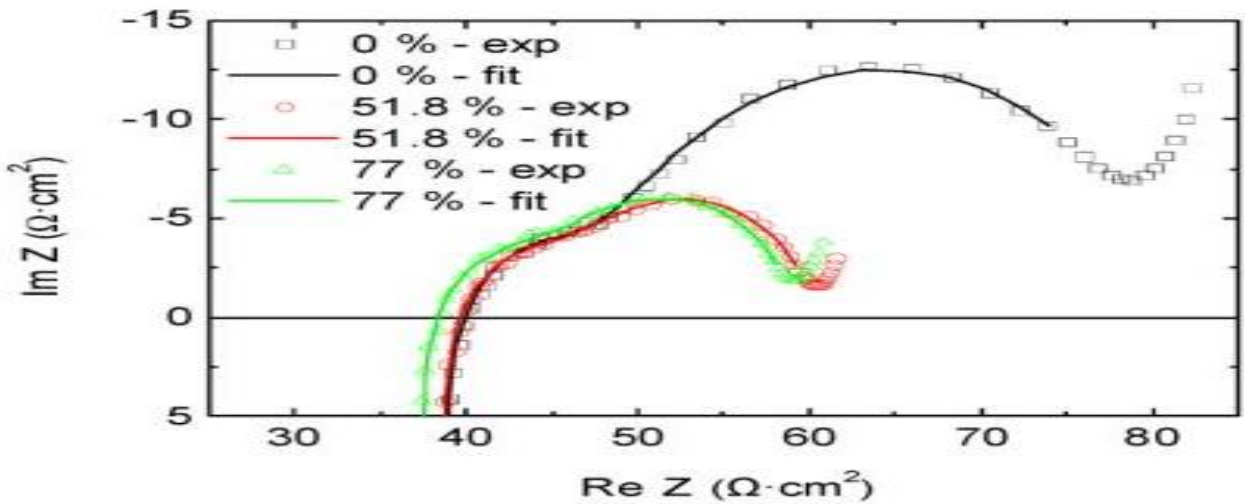


Figure 3.1: [22] Nyquist plot of impedance results obtained from V. Ovejas and A. Cuadras

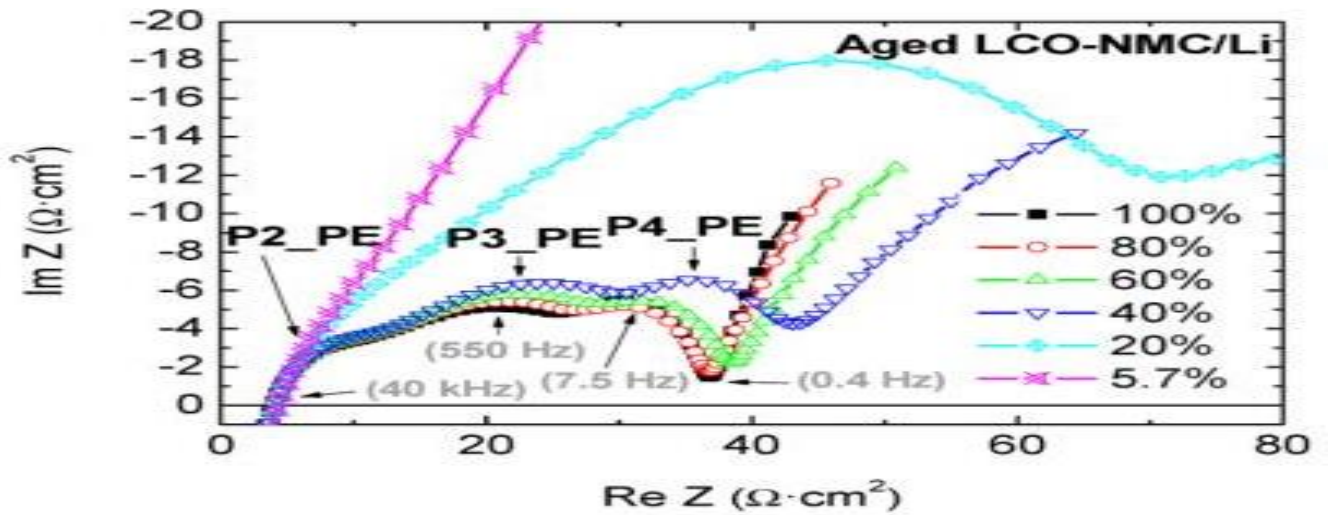


Figure 3.2: [22] Nyquist plot of impedance results obtained from V. Ovejas and A. Cuadras .

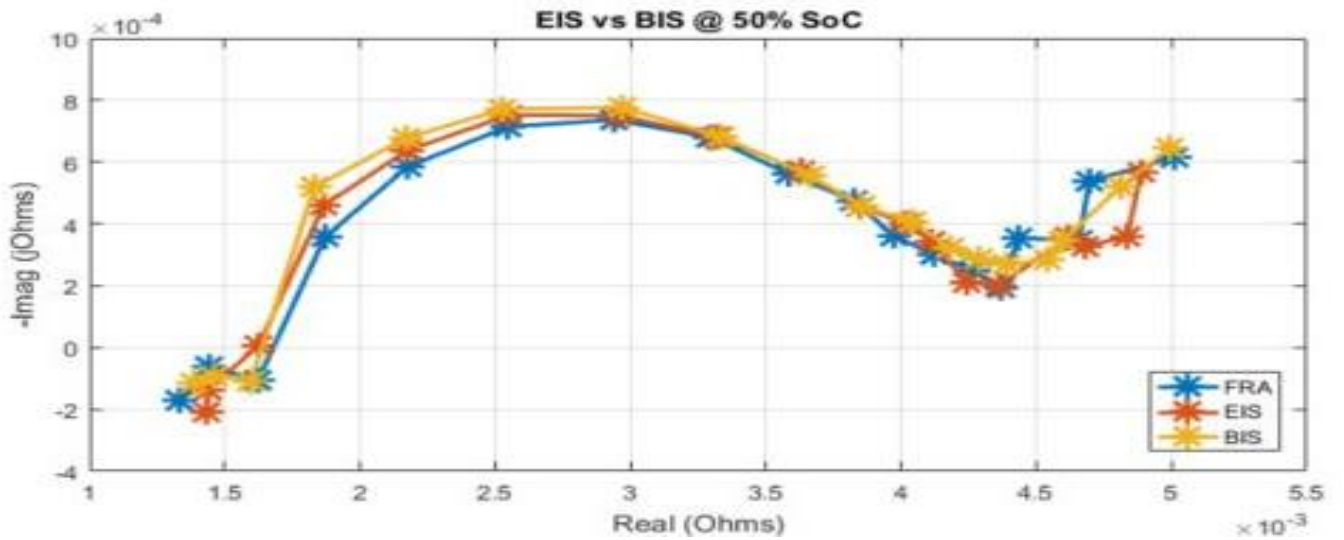


Figure 3.3: Nyquist plot of impedance results obtained from S. Moore [18].

Over a range of values, a Nyquist curve was produced using the impedance equation described in. This served as the benchmark against which following spectroscopic experiments might be evaluated. The code to generate this signal is shown in B3

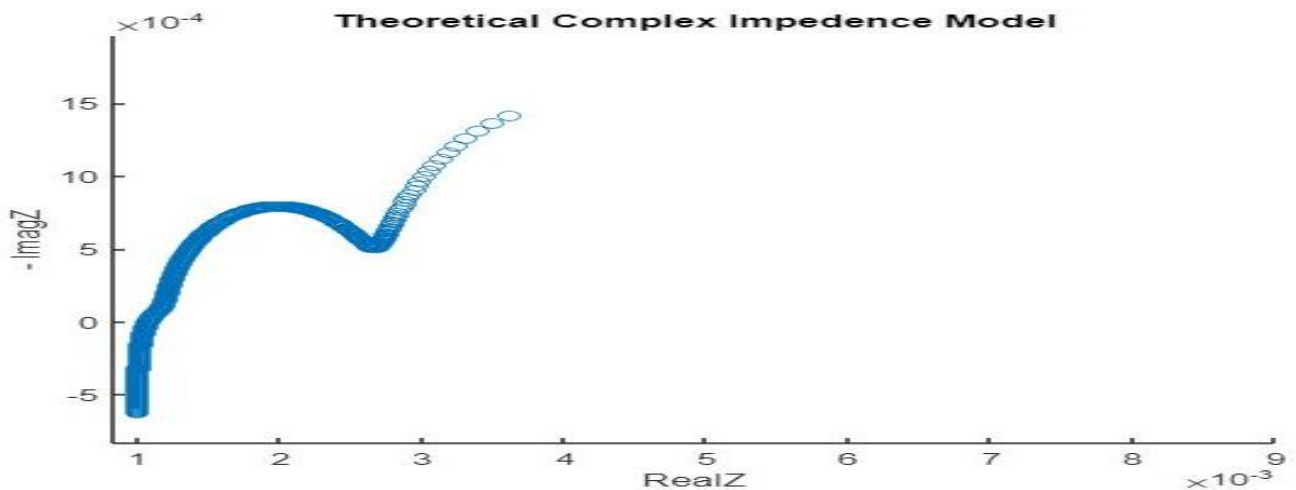


Figure 3.4: Nyquist curve

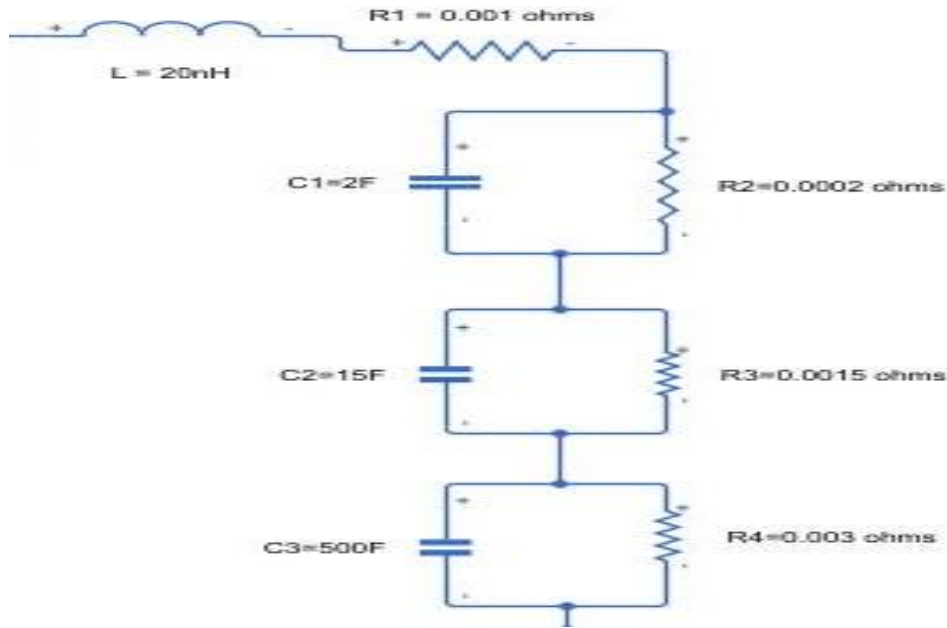


Figure 3.5: Battery Electrical Model

The two figures above represent the theoretically optimum impedance shape based on the numbers displayed in the circuit diagram above.

## Battery's Equivalent Circuit and Electrical Potential (OCV)

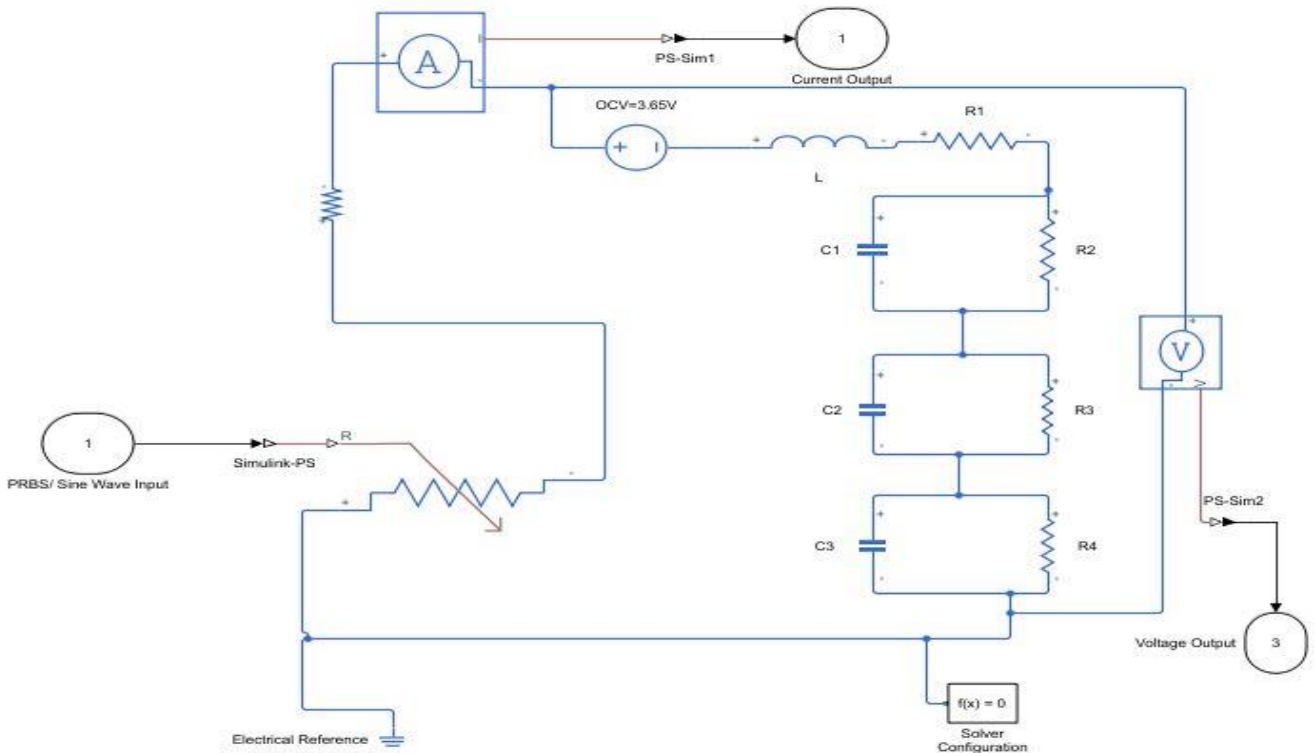


Figure 3.6: The Full electrically equivalent model of the fictitious cell in Simulink.

A straightforward Thevenin battery model was employed in simulation to generate realistic results. The model has one Li-Ion battery that is modelled as a voltage source, an inductor in series with a resistor, three series resistors, and three parallel resistor capacitors that are connected to ground. As a result, in the simulation, the voltage is only measured across the battery model, whilst the current is

measured in series with the battery and the OCV supply voltage. To lessen the computing load on the simulation, this was done. A less complex Li-Ion battery model was also utilized for the simulation for two reasons: first, Simulink does not have more complex components like the Warburg Element, which is present in the majority of Li-ion battery models. The whole Simulink model that was used to represent the hypothetical cell is seen in the picture above.



A 3.65V open circuit voltage was incorporated in the battery simulation model. This corresponds to the cells that were employed in earlier studies by [6, 10, 11]. These "pouch" cells are made of Li (N iCoMn) O<sub>2</sub>. According to [39], 18650 batteries are employed in contemporary, high-performance EVs. Two Sony-produced cells are represented by the cell shown below. As seen in the Figure above, a 3.65V DC voltage source was connected in series with the initial 3rd order Randle circuit in an effort to produce a more accurate simulation model.

**Figure 3.7: 10 Pieces of 3.7 V Volt Rechargeable US18650 VTC5**

## 3.2 Perturbation Signal (EIS and PRBS) in Simulink

### Variable Resistance

Keeping the interference with the load behaviour to a minimum was important when adding a second current signal to the system (PRBS/ EIS). In order to remain inside the linear zone of the cell's performance, the signal needed to be tiny enough. This was first accomplished by connecting a variable voltage source in parallel with the cell model. By adjusting the additional voltage in the pattern of the desired injection signal, it would be simple to control the current in this manner. A complicated and extremely precise power supply would be necessary for such a system, though.

A parallel/series variable resistance would be a more workable design, according to the knowledge gained from physical implementation, which was carried out by [6, 10, 11]. The Simscape component utilized is depicted in the figure below and is connected to an input signal that regulates its series resistance. The risk of "overcharging" the cell is another significant benefit of employing a variable resistance component; if the battery is already at 100% SOC, an additional voltage or current source might push it beyond of its operational limits.

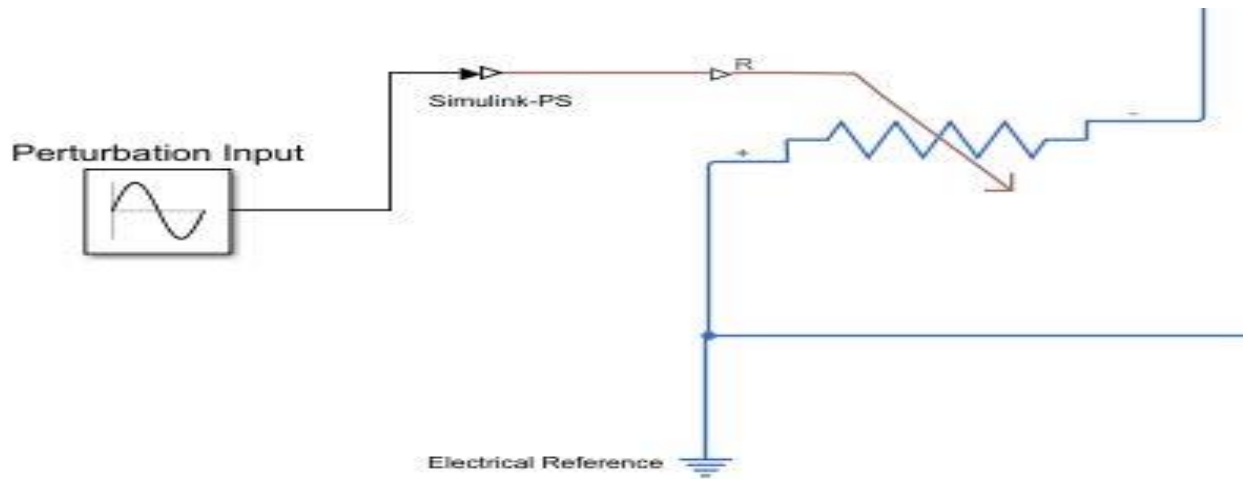


Figure 3.8: A Straightforward variable resistor to regulate signal disturbances flowing through the cell in the Simulink's environment

### 3.2.1 EIS

For the EIS experiments, the following set up was used in Simulink:

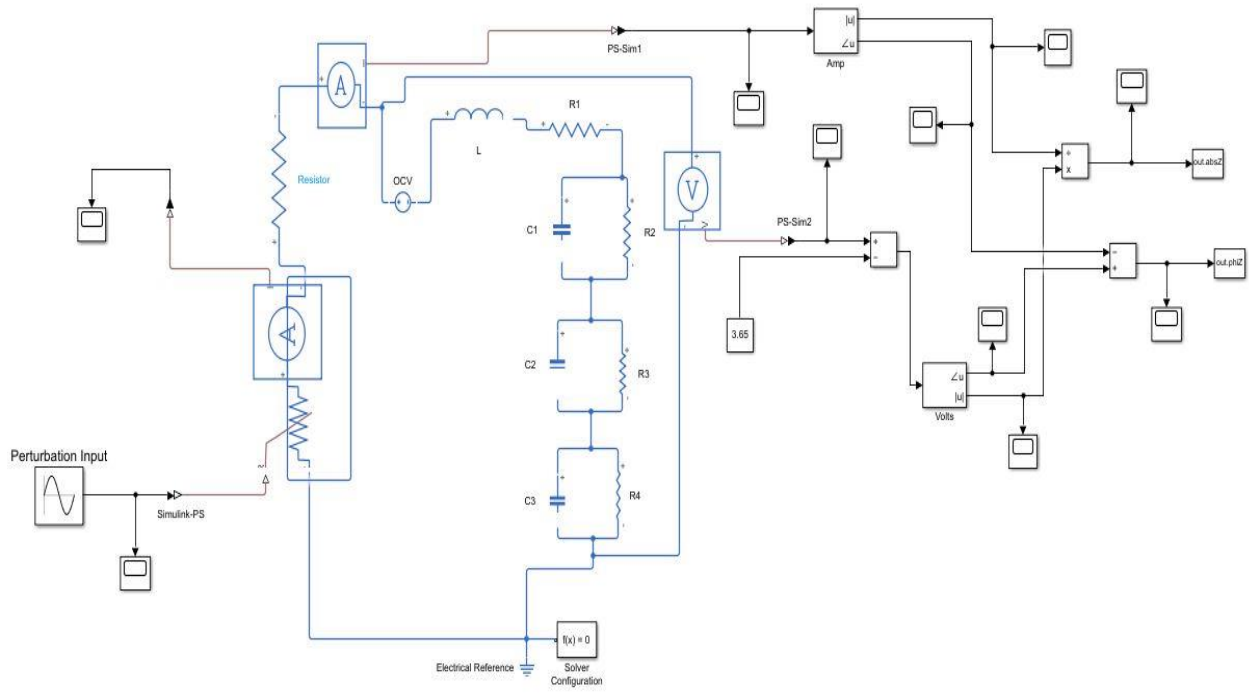


Figure 3.9 The Simulink Circuit used to run EIS Experiments

Electrochemical Impedance Spectroscopy (EIS) entails delivering a succession of distinct sinusoid frequencies through the cell and logging the impedance response for each, as was discussed in the Literature Review section. To emphasize the key regions of the impedance curve, the frequency range and steps between frequencies must be correctly chosen. It was discovered that the whole structure of the selected cell's impedance model, from the diffusion area to its high-frequency inductive end, was sufficiently captured by a frequency range between 0.2Hz and 2680Hz. The second crucial element to take into account was the resolution (i.e., leaps between frequency steps). A curve with insufficient plotting points will be difficult to interpret precisely, while one with too many steps will lengthen the test and perhaps violate the Kramers-Kronig requirements. A rather high resolution of 24 steps was chosen since the predicted curve has two constrained corners (between the diffusion and SEI layer areas). The following equation determined the spacing between each frequency step:

$$frequency = 1.5^n \text{ rad per second}$$

The sinusoids were set up with an amplitude that wouldn't go above 10% of the DC load current flowing into the battery. This required adjusting the extra resistance to get variations that were no greater than 0.375A in the simulation. The series variable resistor was simply set to vary between 0 and 0.1 since the load resistance was fixed at 1 ohm. In other words, between 100% and 110% of the load resistance is represented by the entire resistance in the external circuit. If the cell's internal impedance is tiny enough to be negligible, this procedure is still only an approximation. Depending on the frequency that is being entered, there will be a minor offset.

The EIS perturbation signal fed into the circuit is shown below:

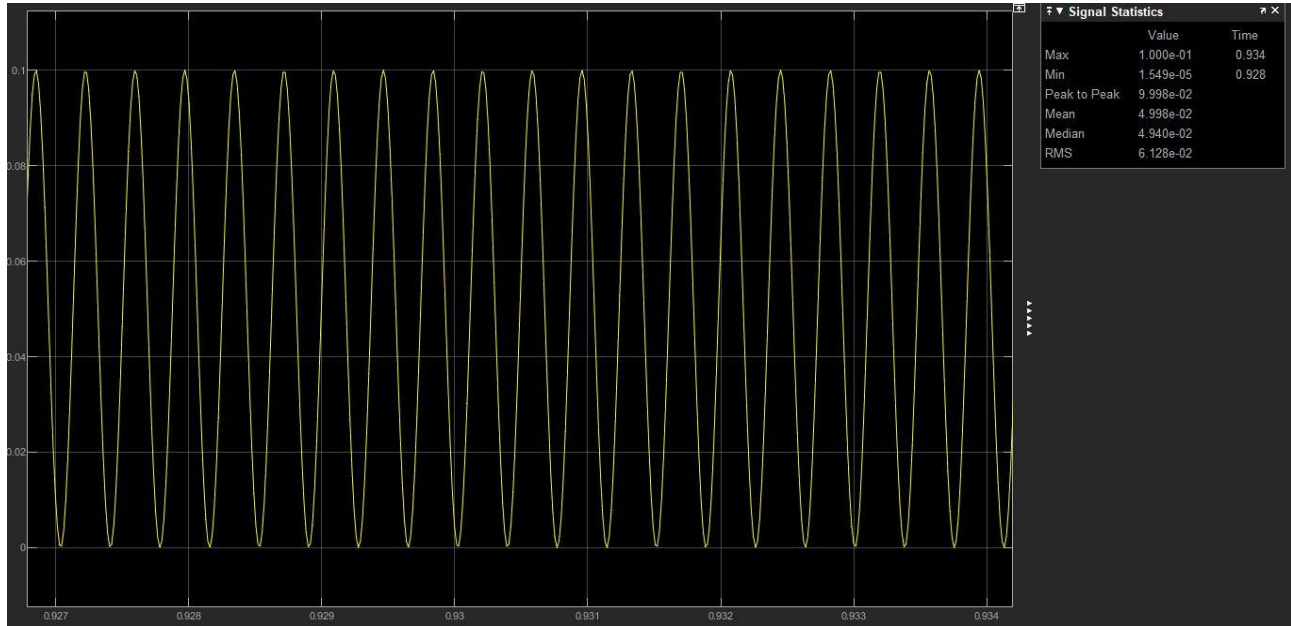


Figure 3.10 The EIS Signal fed into the Circuit shown in [3.9]

## Measurements in Simulation

The current and voltage through and across the cell have to be measured across numerous periods of each perturbation signal injection in order to calculate the internal impedance at each specific frequency. This was accomplished by simply connecting an ammeter block and a voltmeter across the positive and negative terminals of the cell. Both the current and voltage values were then translated to the frequency domain using separate Fourier analysis blocks after adjusting for the DC offset. The computation of Ohm's law was then made from each Fourier transform as follows:

$$Z(j\omega) = \frac{V(j\omega)}{I(j\omega)} = \frac{|V(j\omega)|}{|I(j\omega)|} \angle (\angle V(j\omega) - \angle I(j\omega)) \text{ ohm}$$

Then, using the trigonometric relationships, the polar-form result was transformed to rectangular form to create a Nyquist plot (Real against imaginary components):

$$Z(\text{imaginary}) = Z(\text{magnitude}) * \sin(Z(\text{angle}))$$

$$Z(\text{real}) = Z(\text{magnitude}) * \cos(Z(\text{angle}))$$



The results were averaged over the number of cycles that each frequency perturbation was allowed to run. Once more, a trade-off is necessary: greater precision can be obtained at the expense of a longer test run-time. Fortunately, the benefits of larger sample spaces quickly saturate and disappear. It was discovered that reproducible levels of accuracy were achieved by cycling each frequency injection throughout four to eight sessions. It should be noted, however, that this is an idealized case; bigger averages might help increase the signal to noise ratio for a system with high levels of noise interference.

### 3.2.2 Pseudo Random Binary Signals

For the PRBS experiments, the following set up was used in Simulink:

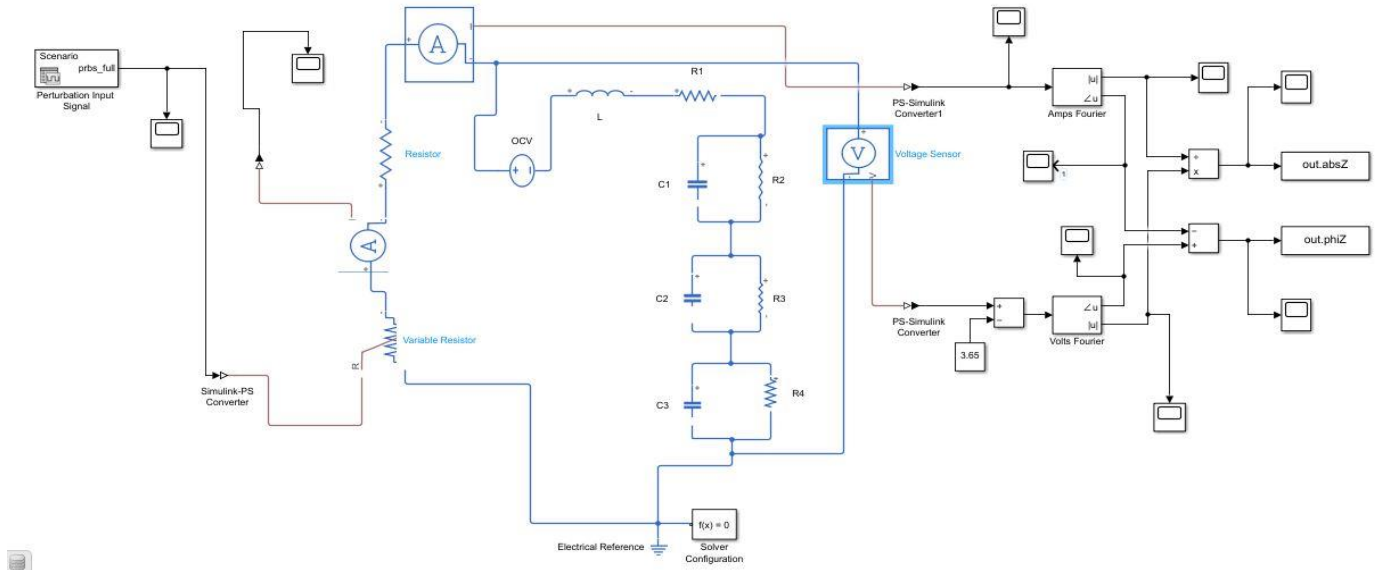


**Figure 3.11 The Simulink Circuit used to run PRBS Experiments**

The EIS methods and the pseudo-random binary sequence testing had a similar basic design, but the input signal makeup and result extraction were fundamentally different. In essence, a PRBS signal is a broadband signal that contains a specific range of frequency components that together make up the random square-wave fluctuations. From 0.2Hz to around 2600Hz, the frequency range doesn't change from the one used in EIS implementation. Each sequence's repetition time and duration are determined by this. The generation frequency regulates length, or the number of bits in each sequence  $f(\text{gen})$ . The generation frequency  $f(\text{gen})$  is chosen to be nearly 2.5  $f_{\text{max}}$  in the figure below. This setting is high enough to provide for a power band that is roughly equal across the frequencies of interest. The fundamental frequency of the signal, abbreviated as  $f(\text{res})$ , is used to indicate the low end of the power spectrum

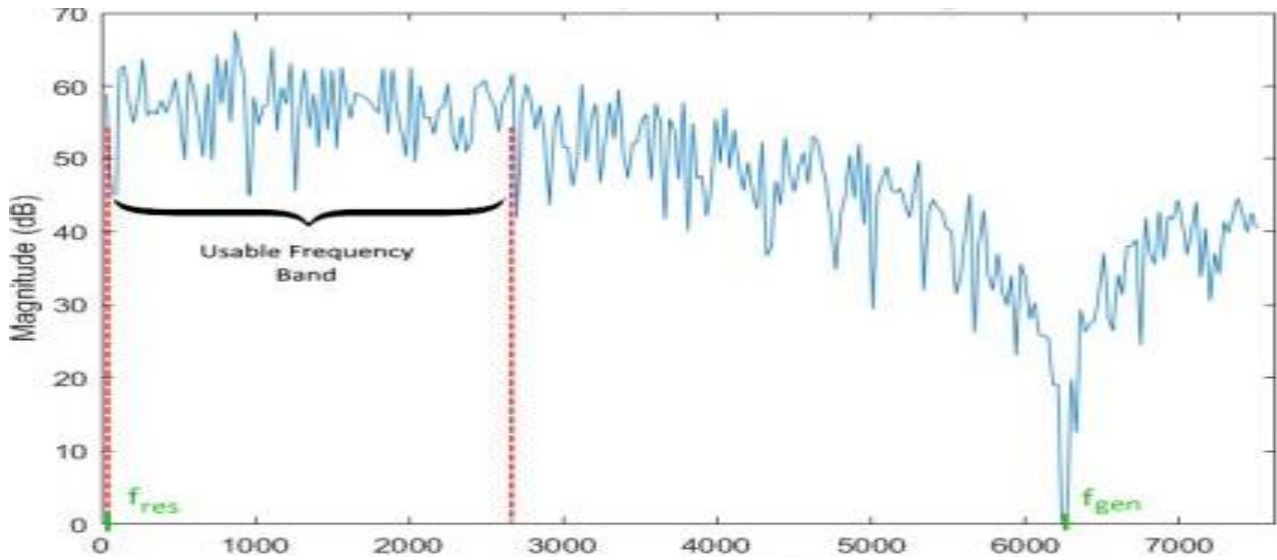


Figure 3.12 Power Spectrum of PRBS Signal over a range of frequencies

The fluctuation period was set and calculated as follows:  $Fluctuation\ period = \frac{1}{f(gen)} = \frac{1}{6300Hz}$

This value evaluates to around 160 seconds. This is related to the power spectrum's zero crossover. The system's sample period must also be small enough to accurately capture the signal. The sample frequency must be at least twice as high as the highest frequency in the signal, according to the Nyquist-Shannon theorem. Given that the PRBS signal contains frequencies infinitely far beyond  $f(gen)$  (of diminishing power), a sample duration of 20 seconds was used. B2 and B1 in the Appendix show the PRBS and EIS analysis code that was implemented.

Also shown below is the PRBS signal that was utilized to create the power spectrum in Figure above.

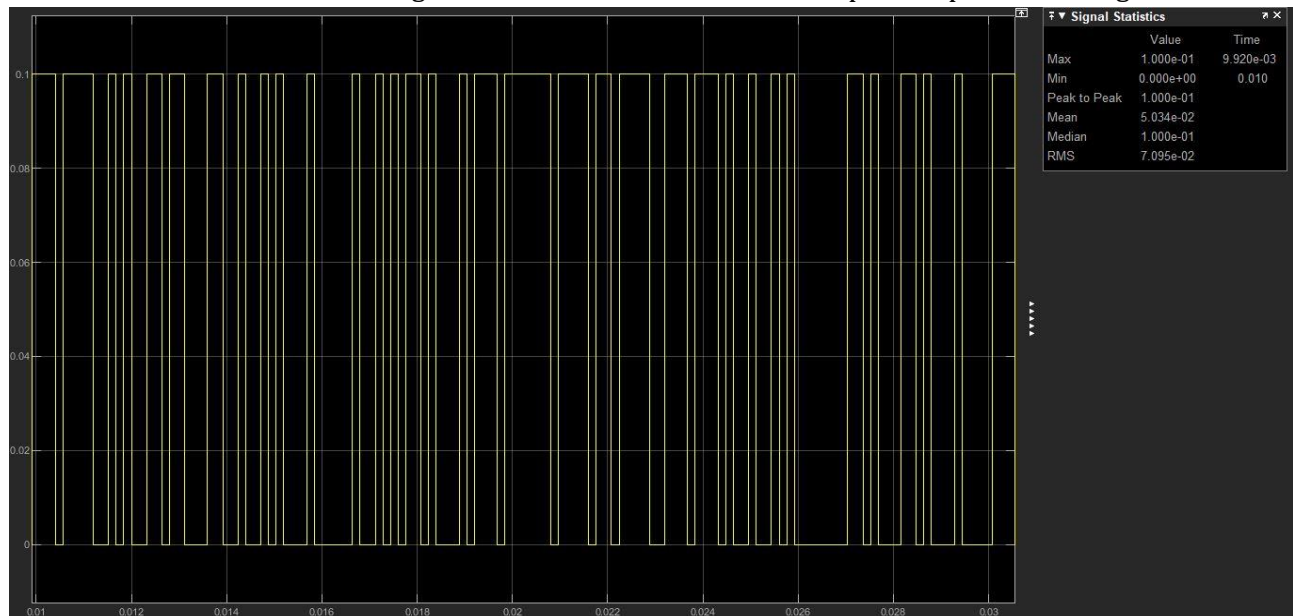


Figure 3.13 The PRBS Signal fed into the Circuit shown in [3.9]

## Measurements in Simulation

The current and voltage measurements were made in series and across the cell, respectively, much like with the EIS process. Each measurement's Fourier analysis took a different route to the EIS.

The entire spectrum of frequencies was recovered at once rather than only analysing one basic frequency component. This was accomplished by creating transforms of several harmonic components with frequencies ranging from the fundamental frequency  $f(res)$  up to the highest interest frequency,



2600Hz. Once more, 24 frequency points were obtained in the sample space. Each point had to be a multiple of the fundamental frequency, which was crucial  $f(\text{res})$ . This may help to explain the naming practice,  $f(\text{res})$ : the more exact the plotting points can be, the lower it is.

The following calculations were used to estimate the precise spacing of these harmonics in order to maintain the EIS method's dispersion. The following calculations were used to estimate the precise spacing of these harmonics in order to maintain the EIS method's dispersion.

$$\text{Frequency Point} = \frac{1.5^n}{2 * \pi} \text{ Hz}$$

$$\text{Harmonic Multiple Factor} = \text{floor}\left(\frac{\text{frequency point}}{f(\text{res})}\right)$$

From the above equation,  $n$  is the index (from 1 to 24),  $f(\text{res})$  represents the fundamental frequency of PRBS.

So, following the calculations based on Ohm's law, the recorded data ( $|Z|$  and  $Z$ ) were stored in two matrices, each of which had 24 columns. Similar to the EIS technique, the findings were then translated from polar to rectangular form before being averaged over each column.

### 3.3 Battery Monitoring Using Impedance Spectroscopy

This research aims to carry out impedance spectroscopy measurements without removing the battery from the system or interfering with system operation. In doing so, the Battery Management System (BMS) will be able to assess the battery's level of charge and modify the battery power management system as necessary using the information gleaned from the impedance measurements conducted online. In the event of a battery failure, information from EIS measurements can be used to identify the failure patterns and underlying causes. For example, battery aging can also be monitored by looking at the changes in the model parameters.

EIS can be done utilizing either linear amplifiers to inject the AC perturbations or the accompanying power boost converter, which connects the battery and the load, to inject signals via duty cycle perturbations. Figure 3.14 illustrates these techniques with the EIS via duty cycle perturbation.

Switching converters can be used for EIS by adding a sinusoidal/ PRBS disturbance to the duty cycle. A typical non-isolated bidirectional dc-dc boost converter that enables the perturbation to be superimposed during the Li-Ion battery's charging and draining is employed. Instead of employing an external linear signal generator, the duty cycle is adjusted. As a result, the duty cycle at time depends on both the perturbation and the steady state duty cycle. This is illustrated below.

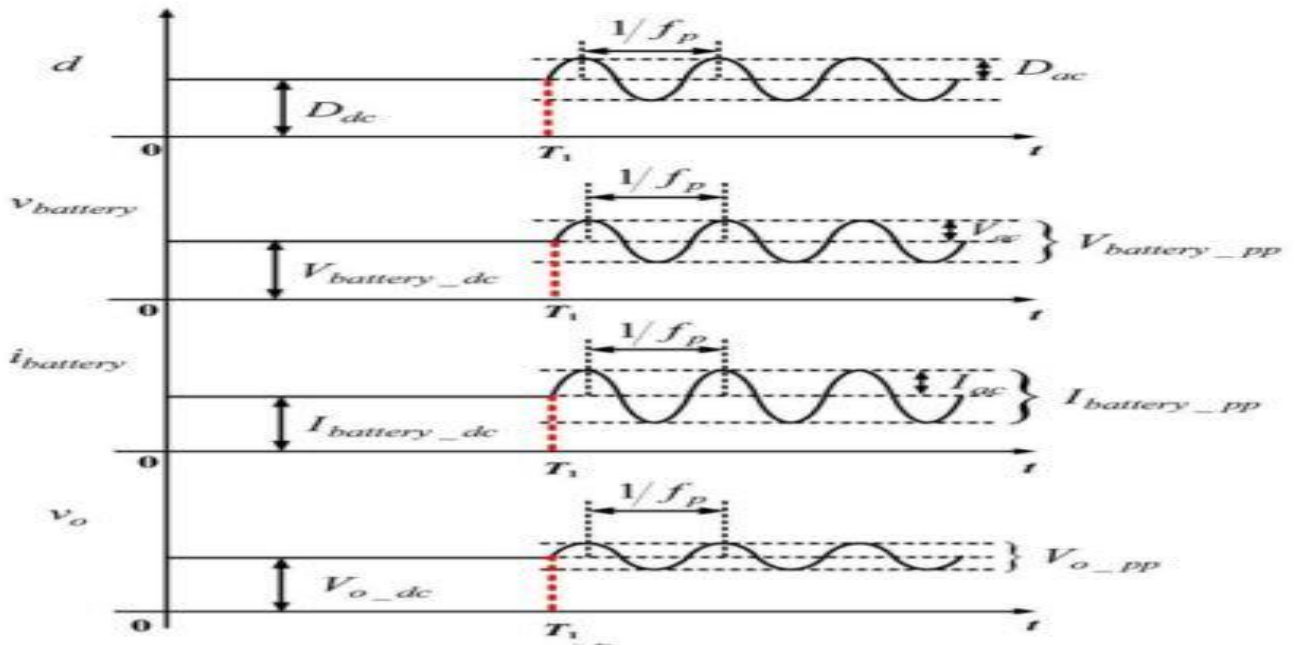


Figure 3.14: Operation of EIS on a Switching Converter

### 3.4 Design Of Perturbation Signal And DC-DC Boost Converter

There are two standard approaches for conducting impedance spectroscopy on a running system, as was covered in Chapter 3.3. The boost converter approach is the way that this dissertation focuses on because it can be used by modifying the power converter and does not require additional power electronics. This technique needs a DC-DC switching converter to be tested.

This section explains the analytical design of the DC-DC boost converter to do IS measurements with its related control, allowing the converter to perform the IS measurements. Additionally bi-directional. These make it possible to test IS techniques in both charging and discharging modes. A simplified systems diagram is shown in Figure 3.15. The battery system is made up a Li-Ion battery pack. Analytical modelling and simulation of the suggested system are the goals of this section.

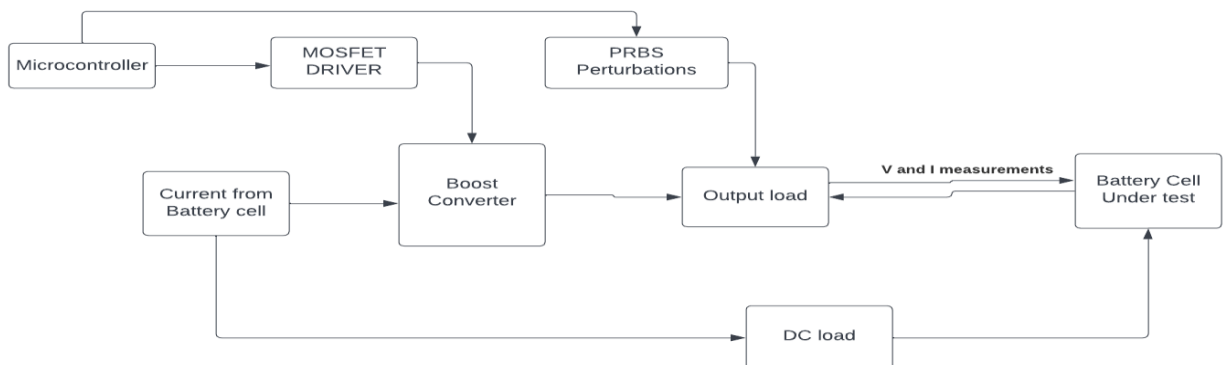


Figure 3.15: System Model

The design of the DC-DC boost converter prototype that will be utilized in experiments serves as the chapter's introduction. By utilizing MATLAB Simulink to simulate the suggested system, the chapter ends. The design of the Perturbation input signal was discussed earlier in section 3.2.

## Analytical Design of Boost Converter

The boost convertor was selected for its ability to follow forward and reverse current operations. This would allow us to perform EIS and PRBS impedance measurements.

While the DC voltage at the load is bucked to a lower value to charge the battery in the reverse current operating mode, the battery voltage is raised and feeds current to the DC output in the forward current operation mode. DC Load at the output of the convertor is treated as a constant resistance whereas the DC Supply tracks the output voltage and will be used as a current source.

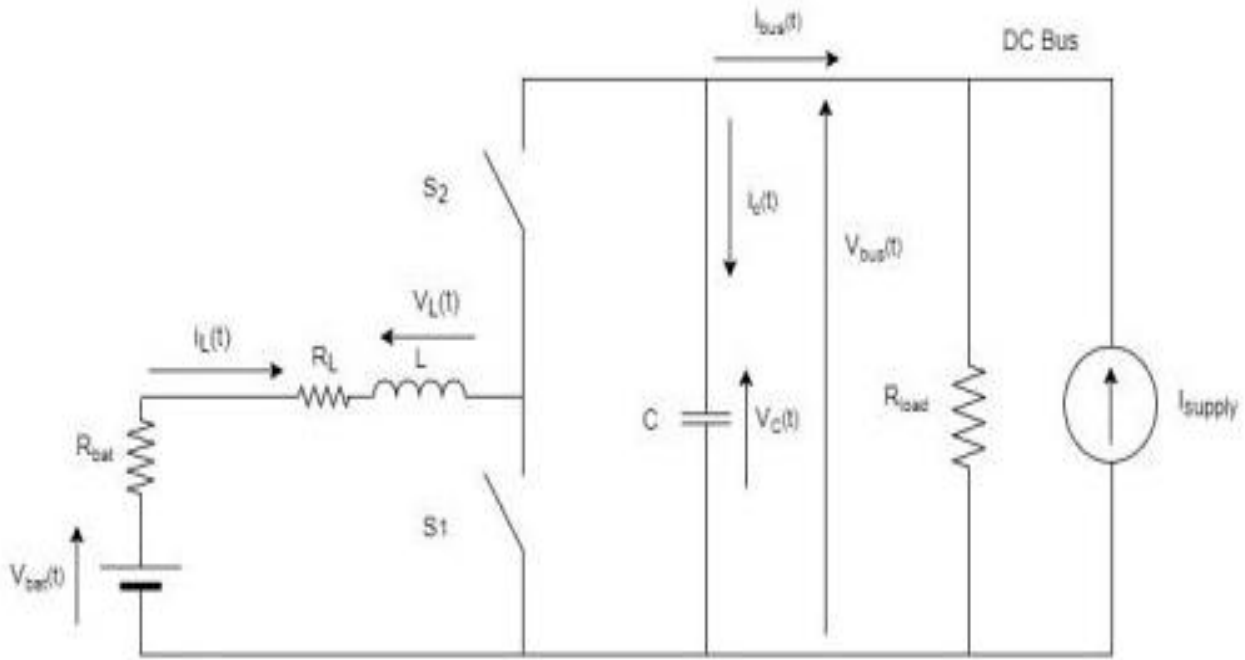
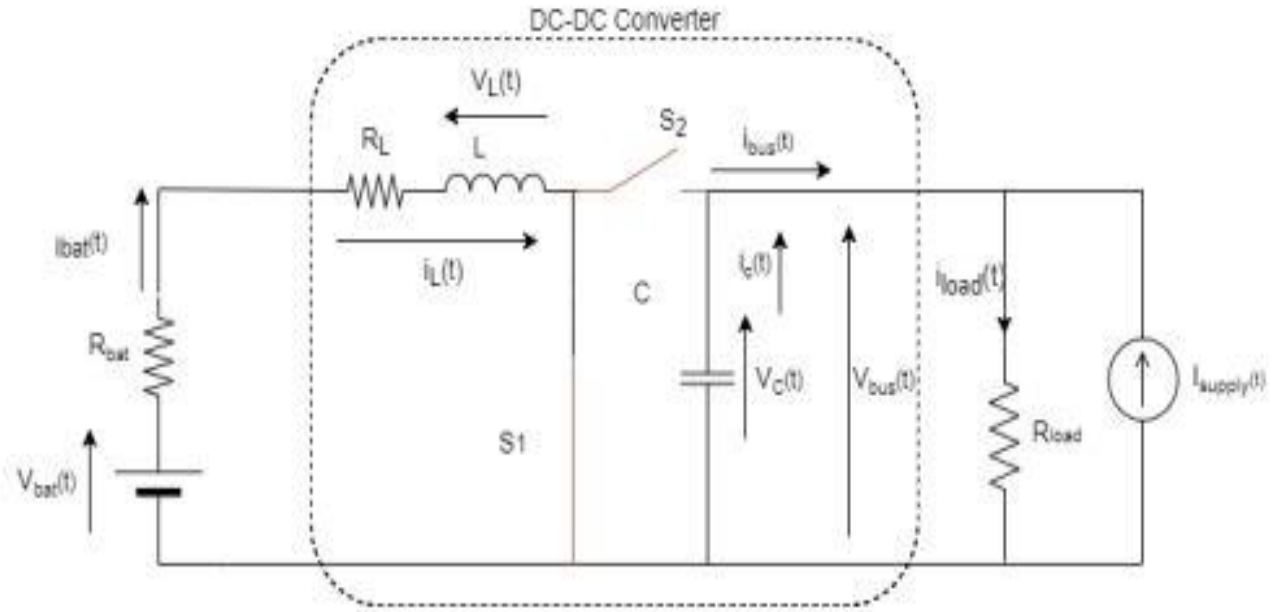


Figure 3.16 The Bi-directional Boost Converter

The switches are controlled synchronously. A technique for controlling several MOSFETs simultaneously is synchronous rectification. A PWM waveform that is 180 degrees out of phase, or when S1 is on, S2 is off, and vice versa, is used to control each of the MOSFETs. As opposed to if the MOSFETs were controlled independently, synchronous rectification is easier to regulate because it does not need figuring out the direction of current flow. Simultaneous rectification of the MOSFETs will be implemented.

First, a mathematical description of the converter's circuit is obtained before modelling it analytically. The first section describes the basic operation for the converter.



**Figure 3.17 Switch 1 ON and Switch 2 OFF on the Boost Converter**

The converter is considered non-linear time variant circuit, due to the inclusion of semiconductors switching elements. Figure following depicts the circuit at time T(on), when S1 is turned on and S2 is closed. S1 links the inductor's output to ground when it is turned on. A voltage  $V(L)$  is established across the inductor as a result. While the inductor currents  $I(L)$  grow,  $V(L)$  steadily declines.  $V(c)$  continuously drops as a result of the discharge of the capacitor through the load resistor. For the circuit in Figure 3.16, when S1 is ON and S2 is OFF, equations are found using Kirchhoff's Voltage Law (KVL) and Kirchhoff's Current Law (KCL)

$$V_{battery}i_L(t)(R_L+R_{battery}) - V_L = 0$$

$$i_c(t) + \frac{V_C(t)}{R_{load}} - i_{supply}(t) = 0$$

The inductor would be connected to the capacitor when S1 is OFF and S2 ON. The capacitor would be charging during this operation and the reverse for the inductor. This means  $V(L)$  will decrease and  $V_C$  would increase.

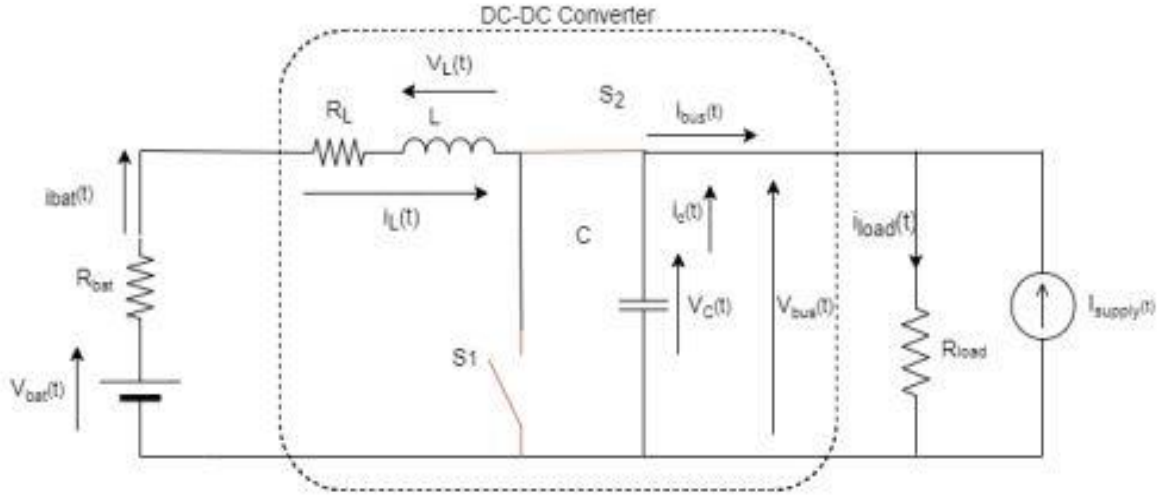


Figure 3.18 Switch 1 OFF and Switch 2 ON the Boost Converter

$$V_{battery}i_L(t)(R_L+R_{battery}) - V_L = 0$$

$$i_c(t) - i_L(t) + \frac{V_C(t)}{R_{load}} - i_{supply}(t) = 0$$

The voltage across the inductor and also the current flowing through the capacitor is described by the following two sets of equations.

$$v_{battery}(t) = L \frac{di_L(t)}{dt} - i_{supply}(t) = 0$$

$$i_c(t) = -C \frac{dv_c(t)}{dt}$$

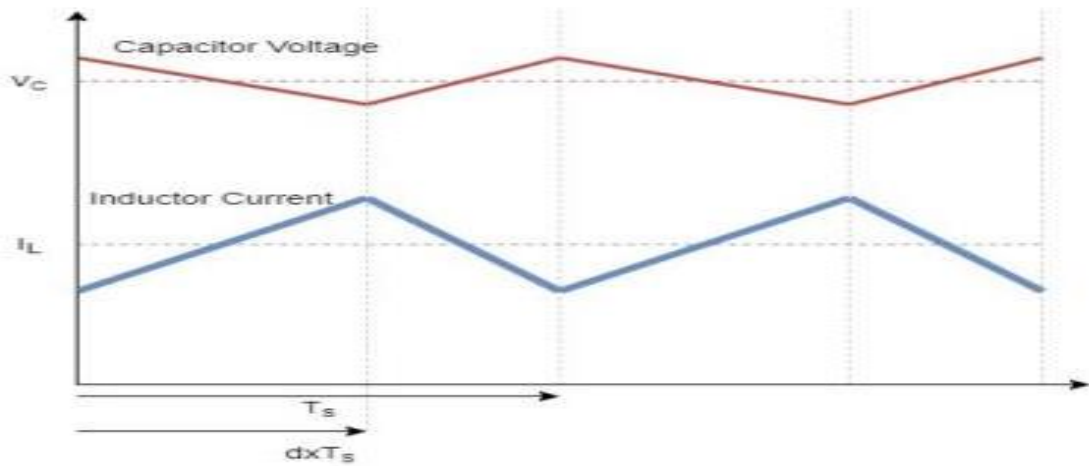


Figure 3.19 Voltage and current waveforms for the capacitor and inductor respectively

Both the average voltage that crosses the inductor and the averaged current flowing through the output capacitor are zero for steady state operation. The DC equations can thus be rewritten as follows

by matching them to zero, realizing that S1 is shut and S2 is opened for (d)Ts, and that S1 is open and S2 is closed for (1- d) Ts.

$$(D)V_{battery} - I_L(R_L + R_{battery}) + (1 - D)(V_{battery} - I_L(R_L + R_{battery}) - V_c)$$

$$(D)I_{supply} - \frac{V_c}{R_{load}} + (1 - D)\left(I_L + I_{supply} - \frac{V_c}{R_{load}}\right) = 0$$

The resistance of an ideal converter's inductor and battery is zero ( $R(L) = 0$ ,  $R(battery) = 0$ ). The formulae below are then used to calculate the equations for capacitor voltage and inductor current. Inductor current  $I(L)$ , output voltage  $V(c)$ , and duty cycle  $D$  have a nonlinear relationship.

$$V_c = \frac{V_{battery}}{1 - D} + \frac{I_{supply}}{(1 - D)^2}$$

$$I_L = \frac{V_{battery}}{R_{Load}(1 - D)^2} - \frac{I_{supply}}{1 - D}$$

The magnitude of the current input on the input determines the direction of the inductor current  $I(L)$ , according to the equations above, assuming that  $V(battery)$ : is positive and that the duty cycle  $\hat{d}$  lies between 0 and 1.  $I(supply)$  is assumed to be a completely generative source, which means it is always positive. If  $I(L)$  is greater than 0, the battery is discharging; otherwise, it is charging. As illustrated in the table below, there are four different operational modes that may take place based on the loading situation and inductor current.

**Table 3.1 Operation Mode of a Converter**

Operation Mode	Inductor Current	Supply Current	Load Resistor
a	Greater than 0	zero	zero < R(Load)< $\infty$
b	Greater than 0	Greater than 0	zero< R(Load)< $\infty$
c	Greater than 0	Greater than 0	R(Load)= $\infty$
d	Greater than 0	Greater than 0	zero < R(Load)< $\infty$

After developing a mathematical model of the bi-directional buck/boost converter, we next choose appropriate component values, filter specifications, and simulation settings.

## Input and Output of the Converter

For the converter, the input and output voltages were chosen to satisfy the required outcome,  $V(\text{battery})$  and  $V(c)$  or output voltage. The values chosen were 4V for the input and 8V for the output side. The input voltage was supplied by a Lithium battery cell of 4V. The minimum battery voltage would be 3V. The power throughout the converter would be in the range of 2.8W.

## The Required Inductor Value

For appropriate buck and boost operation, choosing a suitable inductor is essential. The ripple current in the battery is determined by the inductor selection (and switching frequency). The circuit's  $f_s$ , or switching frequency, was set at 54 kHz. For the purposes of generating sinusoids and PRBS for IS implementation, this frequency is judged adequate. Consequently, by applying the equation below, the ripple current can be calculated.

$$\Delta I_L = \frac{V_{IN} D}{L f_s}$$

It's crucial to make sure that the inductor ripple current is reduced as much as feasible. Since the impedance spectroscopy signals are modulated onto the inductor current, it would guarantee that the inductor continues to operate in Continuous Conduction Mode (CCM) and lessen the ripple current waveform in the battery. The inductor ripple current was chosen to be 0.8A. Consequently, a 2.88 mH inductor was needed. The inductor current must never dip below zero in order to comply with CCM. When the inductor current is equal to half of the inductor ripple current, the discontinuous conduction mode (DCM) and continuous conduction mode (CCM) boundary condition is met.

This means that the boundary condition will occur at:

$$I_L \frac{\Delta_L}{2}$$

When the inductor current goes below zero is when the boundary condition is achieved. The following equation gives this equation.

$$I_{L \text{ boundary}} = \frac{V_{OUT} * D}{2 * L f_s} (1 - D)$$

$$I_{O \text{ boundary}} = \frac{V_{OUT} * D}{2 * L f_s} (1 - D)^2$$

## The Required Capacitor Value

To reduce the output voltage ripple on the output voltage during boost mode operation, an output filter capacitor is necessary. The calculated minimum necessary capacitor value is  $C_{out} = 470\mu\text{F}$ . It was calculated using the formula below.

$$C_{OUT} = \frac{I_{OUT(MAX)} * D}{f_s * \Delta V_{out}}$$

A duty cycle of 0.5 was used. The voltage ripple was set to 0.39V which would be 5% of the output voltage and falls in the required range.

## Driver Circuit for the Converter

According to the block diagram in Figure below, the drive circuitry is in charge of translating the duty cycle into a PWM switching signal and then driving the MOSFETs S1 and S2. The system receives the necessary duty cycle signal, transforms it into a PWM signal with the help of a PWM generator, sends this signal to the MOSFET driver, and then outputs the signal to the high switch and the low MOSFET switches. The generation of the PWM signal will be discussed in detail in the experimental set up section.

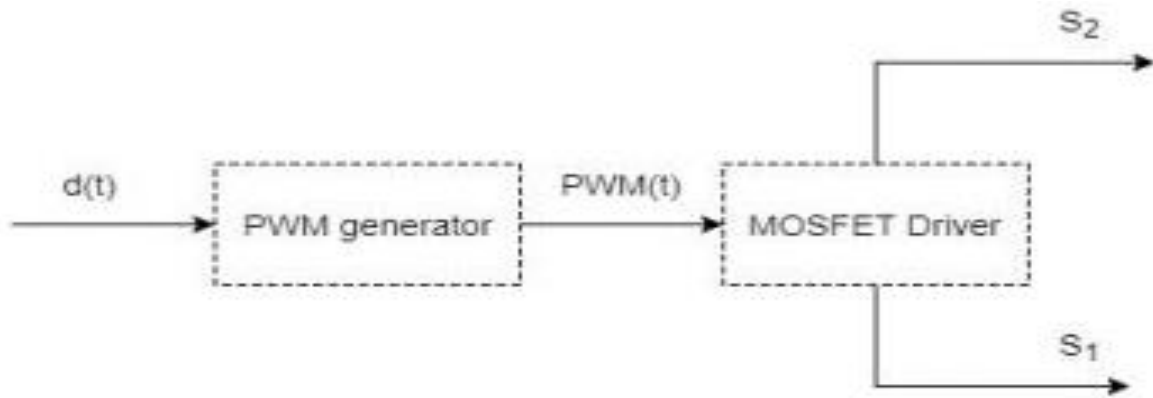


Figure 3.20: Drive Circuitry System



## 4. Experimental Set Up

---

The experimental setup and test procedures for the Li-Ion cells are described in detail in this chapter. In this chapter, one spectroscopic method is considered which is the use of a switching converter for injecting pseudo random signals into the battery, using an electronic load.

The 3.75v lithium-ion batteries were used for the specific experiment. Each cell having a voltage of 3.75v. These were chosen for their better durability. However, to test the properties of the battery, an electrical equivalent circuit was developed which mimicked the battery cells. This is shown in section 3.2 above. In ordinary simple ways, the batteries would need to be charged using a DC power source, to a maximum voltage of 4 V in constant current mode at a rate of 10A. When the current would hit 0.3A threshold value. the cell would be let to rest for 30 minutes to an hour. This condition would be viewed as a 100% State of Charge. The battery would then be put under test.

**Table 4.1: Specifications for the Lithium-ion battery**

Parameter Considered	Specification of Parameter
Cathode	Li [NiCoMn]O <sub>2</sub>
Anode	Graphite based
Nominal Capacity	20Ah
Nominal Voltage	3.65V
Max Voltage	4.15V
Minimum Voltage	3V
AC Impedance	<3m $\Omega$

### 4.1 Building the DC-DC Converter

The converter was required to be constructed in accordance with the guidelines provided in Chapter 3. The building of the DC-DC converter, PWM generation, management of the MOSFETs, and measurement circuits for current and voltage measurements are all covered in this part. The design in Simulink of the bi-directional boost converter is shown in B1.

#### Boost Converter (DC-DC)

A very crucial aspect of the converter is the switches. The IRFP260N International Rectifier Power MOSFET, 5th generation, was selected as the MOSFET. This MOSFET can handle 50A of current and has a reduced on-state resistance of 0.04 Ohms. The IRFP260N family of high voltage MOSFETs is a new generation that uses a cutting-edge charge balance mechanism for exceptional low on-resistance and lower gate charging capability. The Figure below shows the set-up of the bi-directional converter in the laboratory.

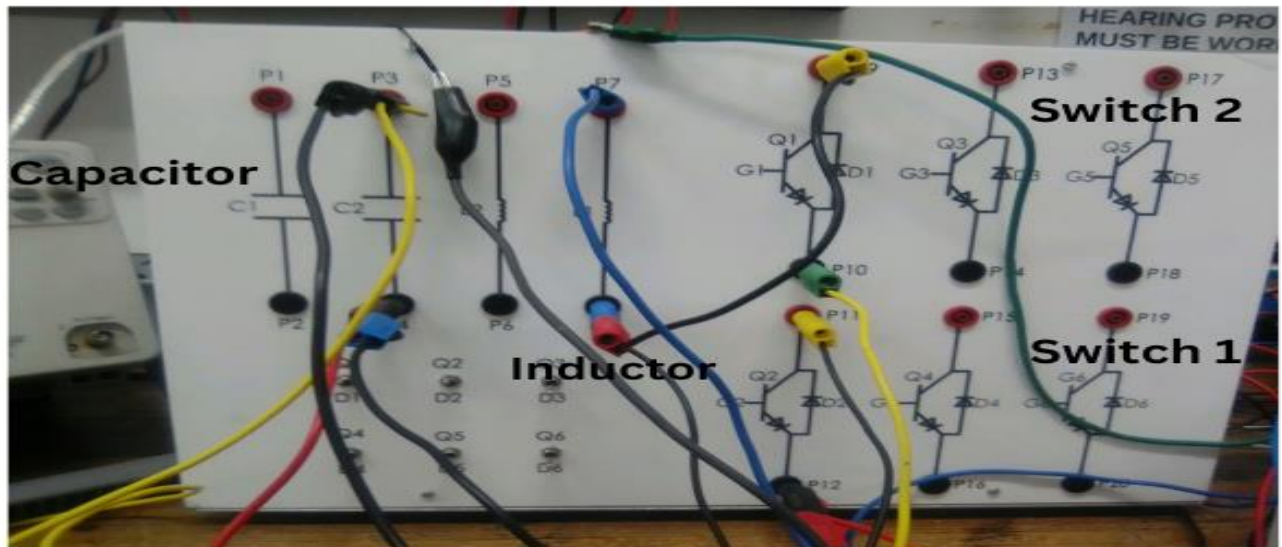


Figure 4.1:Bi-directional Boost converter

The inductor value: 2.88Mh

The capacitor value: 470micro Farads

## Generation of PWM and Pin Connection

There are two ways to create a PWM signal: either analogue circuitry or digitally using a microcontroller. The proposed method was the use of a microcontroller.



Figure 4.2: LAUNCHXL-F28379D Launchpad

The microcontroller used was the LAUNCHXL-F28379D. This is an all-inclusive, budget-friendly development board for Texas Instruments Delfino™ F2837xD devices. The LAUNCHXL-F28379D development kit comes with all the hardware and software required to create programs based on the F2837xD microcontrollers. Once the design requirements are determined, this Launchpad, which is based on the superset F28379D device, enables users to quickly move to lower feature set and/or lower pin count F2837x devices. It has a built-in JTAG debugging tool that enables easy programming, debugging, and testing via a direct PC interface. The USB interface offers the F28379D device a UART serial connection to the host PC in addition to JTAG emulation.

The Figure below shows how MATLAB/Simulink was used as an interface to communicate with microcontroller. The parameters set are shown below as well.

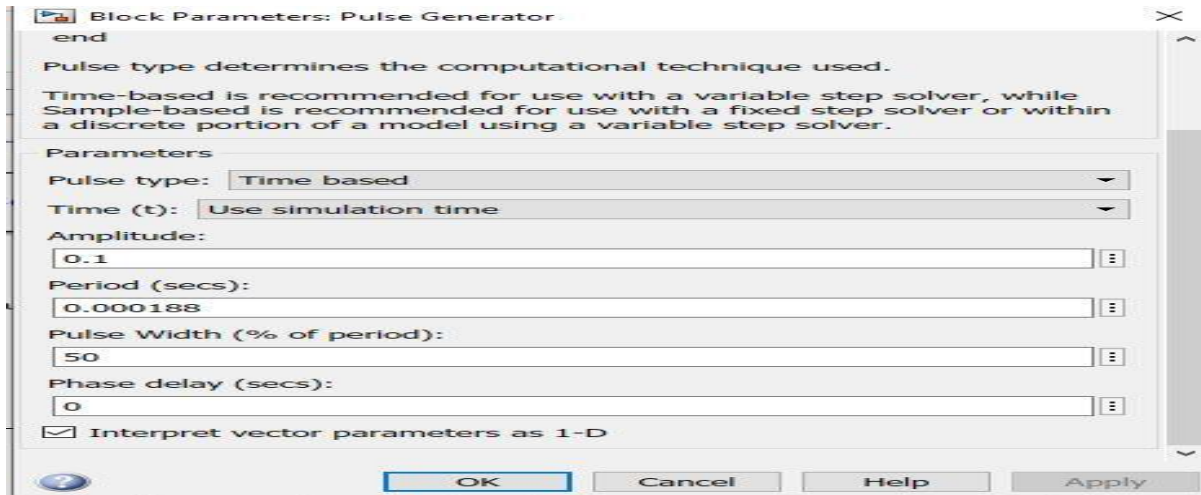


Figure 4.3: Block Parameter for PWM Generation

The duty cycle was set to 50%. Which means that the output of  $V(\text{out})$  would be twice  $V(\text{in})$ . The values of  $V(\text{out})$  and  $V(\text{in})$  were specified in section 3 of this report. The period was set to 0.0000188 seconds which is a frequency of 54kHz. These values were chosen so as to obtain the desired output voltages and currents. The calculations were shown in section 3 of the report.

The pulse was generated in Simulink using Pulse Generator shown in the Figure 4.3. The Figure below shows how the signal was loaded onto the microcontroller. GPIO pins (00 to 01) or ePWM (1A-7A and (1B -7B)) where the output ports could have been used. For pin out connections, two PWM signals were fed to GPIO pin 40 and 39 respectively.

U14D		
GPIO12	C2	GPIO12/EPWM7A/CANTXB/MDXB/EQEP1S/SCITXDC/UPP-ENA
GPIO11/PWMOUT6B	C1	GPIO11/EPWM6B/SCIRXDB/OUTPUTXBAR7/EQEP1B/UPP-START
GPIO10/PWMOUT6A	B2	GPIO10/EPWM6A/CANRXB/ADCSOCBO/EQEP1A/SCITXDB/UPP-WAIT
GPIO9/PWMOUT5B	G3	GPIO9/EPWM5B/SCITXDB/OUTPUTXBAR5/EQEP3/SCIRXDA
GPIO8/PWMOUT5A	G2	GPIO8/EPWM5A/CANTXB/ADCSOCBO/EQEP3S/SCITXDA
GPIO7/PWMOUT4B	B6	GPIO7/EPWM4B/MCLKRA/OUTPUTXBAR5/EQEP3B/CANRXB
GPIO6/PWMOUT4A	A6	GPIO6/EPWM4A/OUTPUTXBAR4/EXTSYNCOUT/EQEP3A/CANTXB
GPIO5/PWMOUT3B	D7	GPIO5/EPWM3B/MFSRA/OUTPUTXBAR3/CANRXA
GPIO4/PWMOUT3A	C7	GPIO4/EPWM3A/OUTPUTXBAR3/CANTXA
GPIO3/PWMOUT2B	B7	GPIO3/EPWM2B/OUTPUTXBAR2/MCLKRB/OUTPUTXBAR2/SCLB
GPIO2/PWMOUT2A	A7	GPIO2/EPWM2A/OUTPUTXBAR1/SDAB
GPIO1/PWMOUT1B	D8	GPIO1/EPWM1B/MFSRB/SCLA
GPIO0/PWMOUT1A	C8	GPIO0/EPWM1A/SDAA

Figure 4.4: LAUNCHXL-F28379D Output ports

These signals were fed into the two MOSFETS of the boost convertor. Each MOSFET is driven by a PWM waveform that is 180 degrees out of phase, i.e., when S1 is on, S2 is off, and opposite. Since the direction of current flow does not need to be determined, synchronous rectification is easier to regulate than independent MOSFET control. The function block shown in the Figure below was used to invert the other PWM signal.

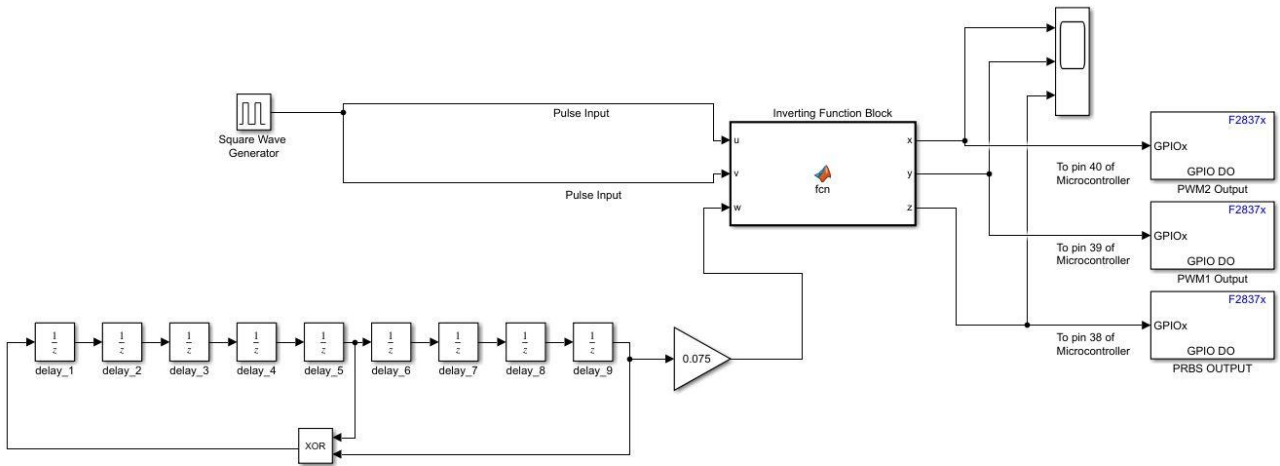


Figure 4.5: Interface between Simulink and LAUNCHXL-F28379D Launchpad

## 4.2 PRBS Signal Generation and Sinusoidal Generation

### PRBS Generation

This part of the report covers the generation of PRBS signal as well as the sinusoidal signal for injections. Same as the PWM generation. The same was done for PWM. The only difference being that a pseudorandom binary sequence (PRBS) is a repetitive, deterministic signal that oscillates between two values and has characteristics similar to white noise. The maximum period of a PRBS signal, whereby  $n$  is the PRBS order, has a built-in periodicity of  $2n-1$ .

The signal was generated using two methods. The 1<sup>st</sup> method involves using a Model Linearizer in Simulink or the command line. The estimation algorithm injects the signal and measures the response at the output analysis point.

The following parameters were specified:

**Amplitude of signal-** This was the peak-to-peak range of the signal, and it was set to 0.075. This specific value was chosen for the same reason mentioned in chapter 3. The input perturbation injected into the system needs to be within 10% of the DC load current through the battery. The cell used had a voltage of 3.75V. The load across the battery was 5 ohms. Hence this evaluates the DC current to 0.75A.

**Sample time-** This was set to match the sample time at the signal for the input and output signal analysis.

**Signal Order-** The PRBS signal can be as long as  $2n-1$ , where  $n$  is the signal order.

**Number of Periods-**  $N_p$  is the number of periods for every frequency

The frequency range as mentioned earlier was from 0.2Hz to 2680Hz. Our system is a discrete time system, the following equation was used to calculate the order of our signal:

$$n = \left\lceil \frac{\log\left(\frac{2 * \pi i}{T_s * 0.2}\right)}{\log(2)} \right\rceil$$

$$T_s = \frac{2 * \pi i}{5 * 2680}$$

The Figure below shows the calculated values being entered in Simulink to generate the PRBS signal

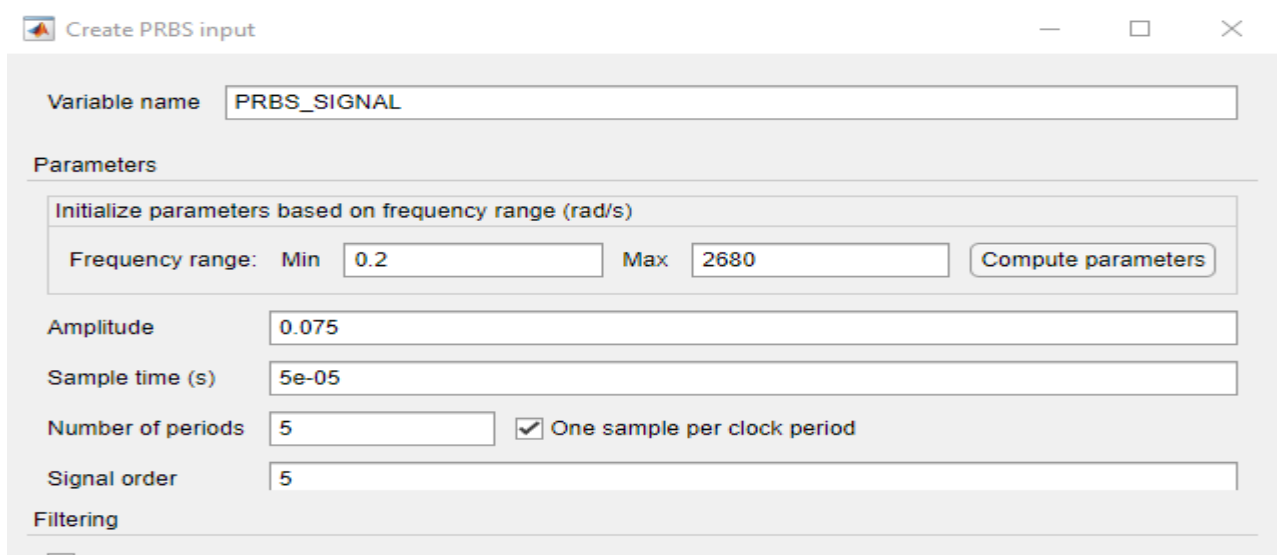


Figure 4.6: PRBS generation in Simulink

The 2<sup>nd</sup> method for the PRBS signal involves the use of delay block in Simulink. The Figure below shows how this circuit was built. The amplitude of the signal perturbation was set to 0.075 for the same reason mentioned in the 1<sup>st</sup> design method.

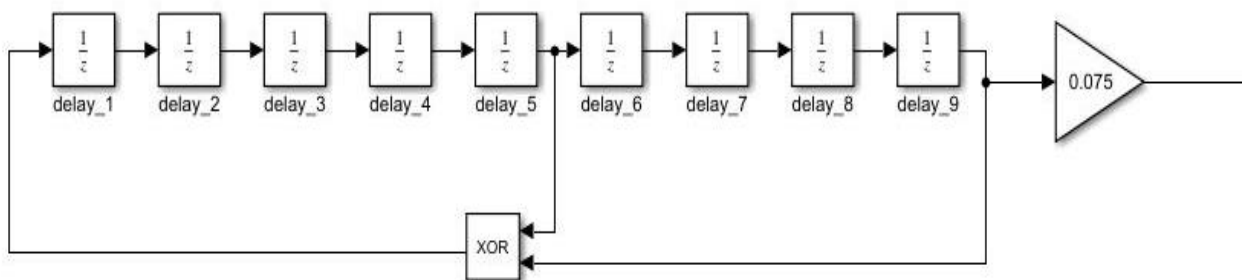


Figure 4.7: PRBS Generation using a 9-bit circuit

## PRBS Output

The output signal from the scope was measured using a DSO6012A signal oscilloscope with a frequency range of 100 Mega Hz. The figure below shows the generated ORBS signal that was injected into the battery cell through the boost converter.

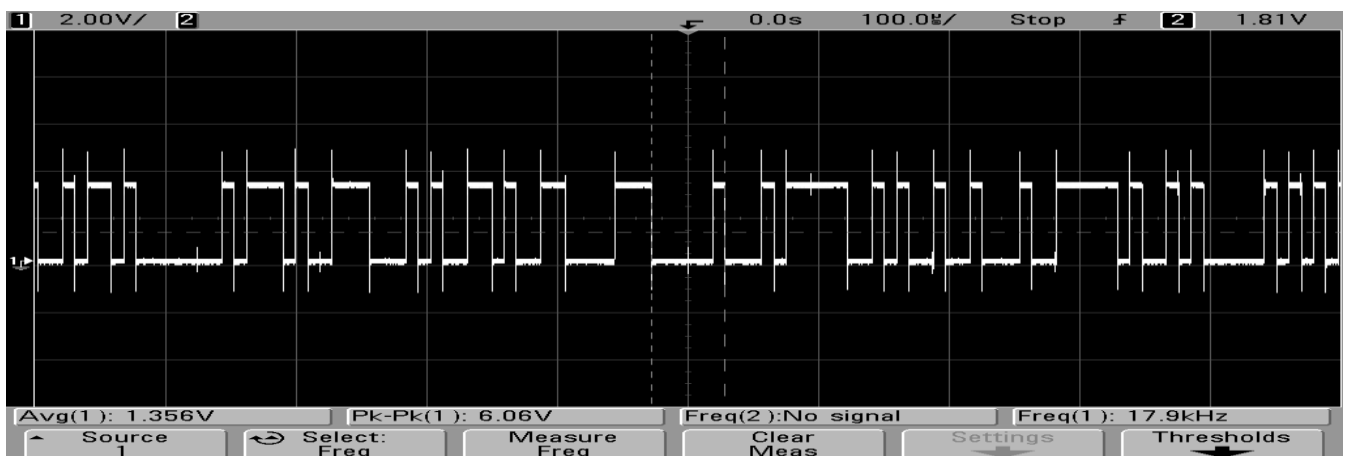


Figure 4.8: PRBS Signal Output



## Sinusoidal Generation

The sinusoidal signal for EIS measurements was produced using signal generator oscilloscope. A 3320A 20Mega Hz function generator was used for producing this perturbation signal. The figure below shows the generator.

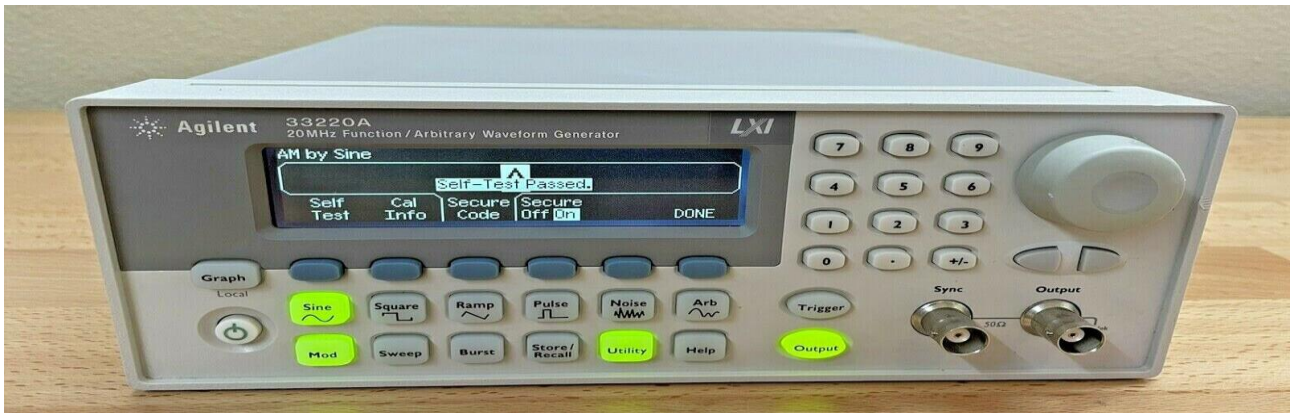


Figure 4.9: 3320A 20Mega Hz function generator

A 20 MHz synthetic function generator with integrated arbitrary waveform and pulse capabilities is the Agilent Technologies 33220A.

This function generator offers bench-top and system characteristics, making it a flexible option for your testing needs and electrical applications. Although it has a low power output, the generator was suitable for this thesis.

To produce the desired sine wave, certain parameters were initially set.

**Freq-** This was manually changed according to the values in the following.

**Ampl-** This is the peak-to-peak value of the signal, and it was kept to a constant value. Only the frequency was adjusted after every injection. The amplitude again was set to 0.075.

**Offset-** This is the DC voltage. It was set to zero in order to centre our signal at the 0 value

**Width-** This is the width of the pulse waveform

**Duty Cycle-** This determined the duration of the pulse.

## Sinusoidal Output

The Figure below shows the output waveform from the signal generator

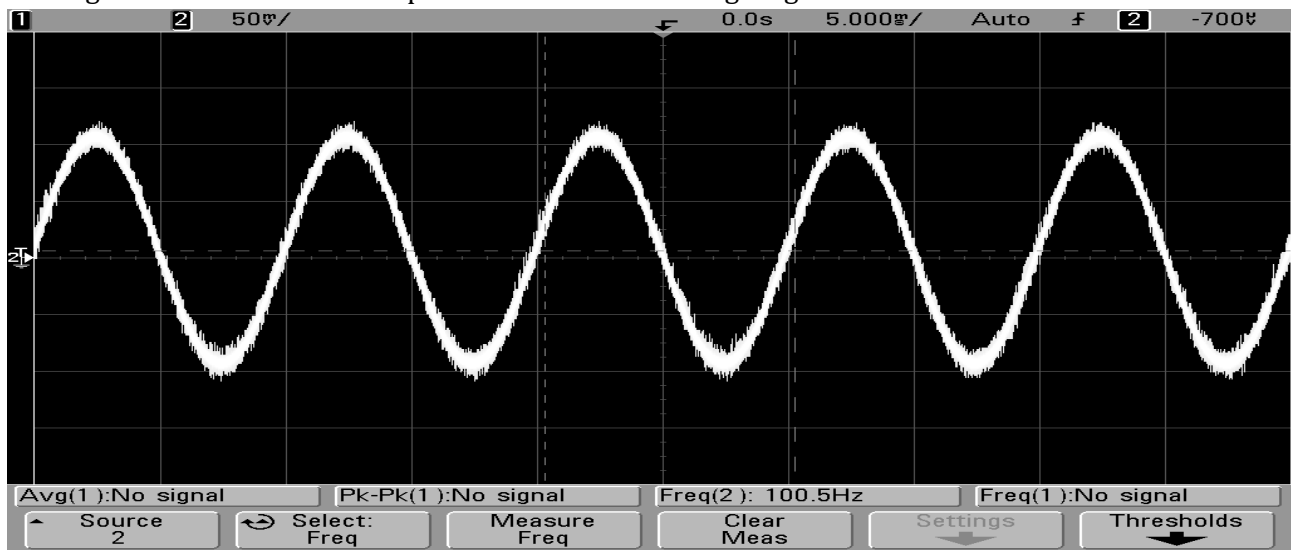


Figure 4.10: Sinusoidal Perturbation from Function generator

## Driver Circuit for the Converter

Due to the synchronized driving of the MOSFETs, the PWM waveforms utilized to switch the two switches are mirror images of one another. The issues that come with this arrangement are numerous. First, it should be confirmed that S1 and S2 are not turned on simultaneously. This situation is referred to as "shoot through," therefore there needs to be some "dead time" between switches. The second problem is that a voltage higher than the source is required to turn on the high-side switch S2 drive. To achieve this, the following circuit was used.



Figure 4.11: Mosfet Driver with two Transistors

The BJT's are named Q1 and Q2. They are both powered by the input voltage of 3.75V. This circuit was designed in such a way that Q1 and Q2 are not on at the same time. The NOT gate was implemented to invert the signal (PWM) from the microcontroller into Q1 and invert it again into Q2. In other words, when Q1 is high, Q2 is LOW and vice versa.

## 4.3 Current and Voltage Measurements

A current and voltage transducer measures current and voltage. Three system variables must be measured for a full IS operation (PRBS and EIS) utilizing the switching converter: the output voltage  $V(c)$ , inductor current  $I(L)$ , and each battery voltage  $V$ . (battery). The circuitry created for these measurements is described in depth in this section.

### 4.3.1 Measurement of Inductor Current

Using a current transducer, the inductor current  $I(L)$  was determined. It uses the Hall effect to measure current. It requires a supply voltage of  $\pm 15V$  and has a conversion ratio of 1:1000. At the module's output, a 1 k ohm resistor was utilized to create a voltage that represents the current. This meant there was a 1:1 relationship between voltage that was measured and current. i.e., when the inductor current equals 0.5A, a voltage of 0.5V appears across the output.

### 4.3.2 Voltage Measurement

The voltage level  $V(c)$  and the battery voltage  $V(\text{battery})$  are the voltages of importance. The voltages had to be collected by the NI-DAQ. A voltage divider was employed to scale down the reading for  $V(c)$  so that it could be measured at the converter's end. The set up for this project had 2 battery cells. One cell was used to power the battery and the other one to receive perturbation signals from the converter.

### 4.3.3 Implementation of the Bi-Directional Converter Overall

The figure below shows the overall layout of the system implemented.



Figure 4.12: Boost Converter

The connections into and out of the converter are shown in the Figure below. The inductor is connected to the 3.75V. The lithium-ion cell was used instead of a direct DC supply so as to allow injection of perturbation signals into the battery. The inductor then connects to the two switches labelled as Q1 and Q2. The 1<sup>st</sup> Switch is connected to the ground, to the 2<sup>nd</sup> switch, the driver circuit as well as the microcontroller to receive PWM. The driver circuit cannot be seen at this angle. Figure 4.14 will show both the driver circuit and the microcontroller. The 2<sup>nd</sup> switch is connected to capacitor of the convertor where  $V(c)$  will be measured. The  $I(L)$  inductor current is measured at the output of the inductor connected to the battery.



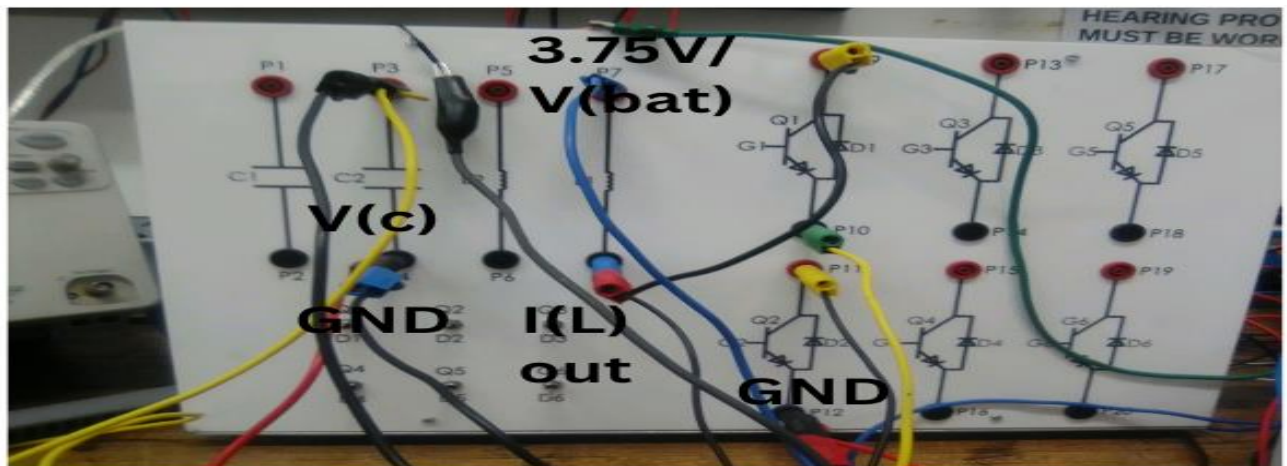


Figure 4.13: Front view of the boost converter

The Figure below shows the Driver circuit and microcontroller implemented.



Figure 4.14: Mosfet Driver and F28379D Launchpad

The batteries used were 3.75 Li (NCoMn)O<sub>2</sub> cells. One cell was used as voltage source for the convertor and the other one was used for EIS and PRBS Impedance measurements tests. The Figure below shows this cell.

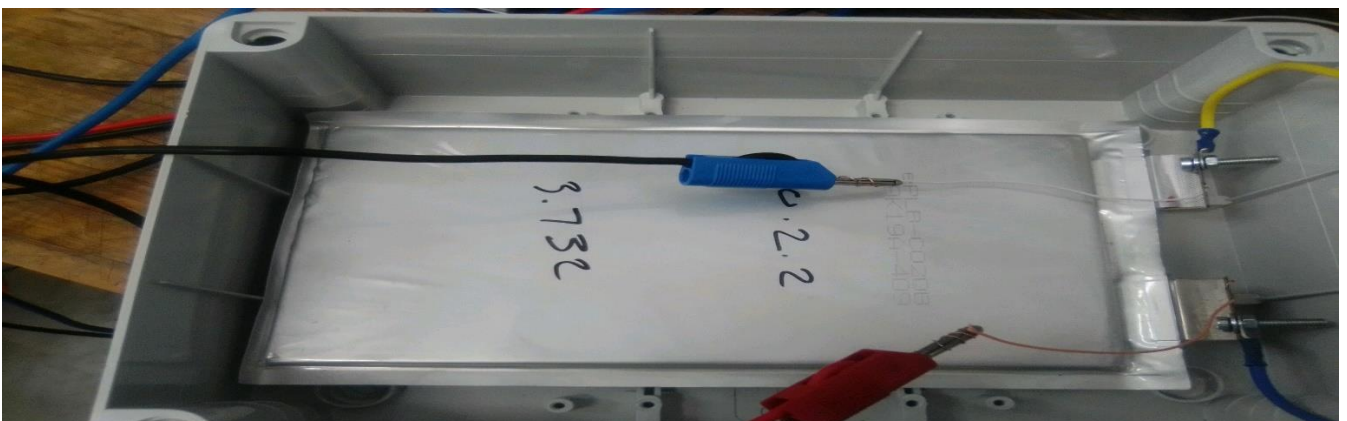


Figure 4.15: Li (NCoMn)O<sub>2</sub> Cell

In order to safeguard the converter from harm brought on by overcurrent/overload or short circuit, a circuit breaker electrical switch was attached to the battery (between the battery and the boost converter). Its primary purpose is to halt current flow when protective relays identify a defect. The Figure below shows the connection breaker to the circuit.

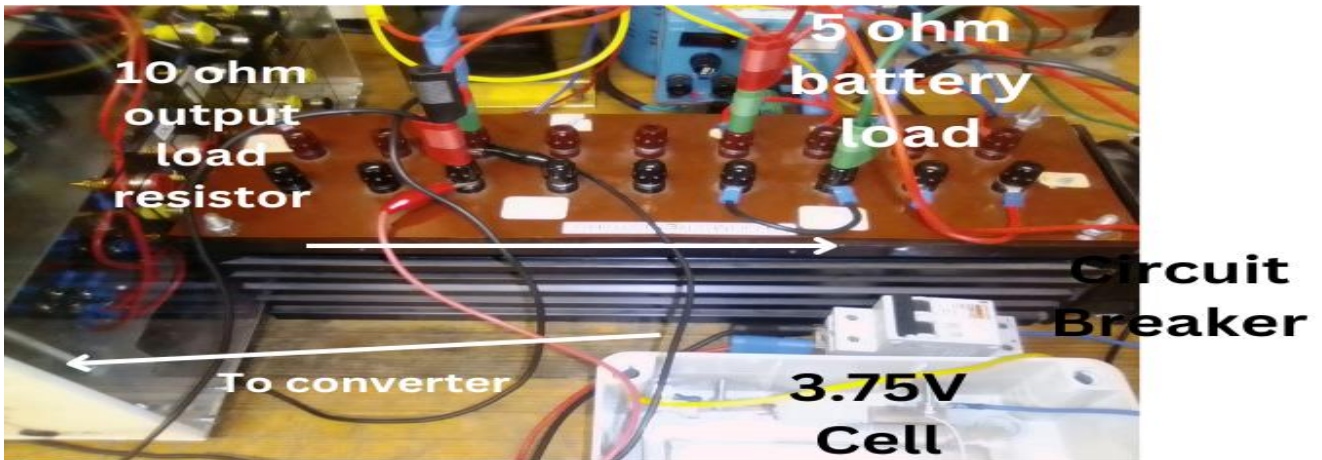


Figure 4.16: Experimental Set of the battery and circuit breaker

## 4.4 EIS and PRBS on Switching converter

The methodologies used on the dc converter during testing are outlined in this section.

### Setup of the Experiment

The set up for the project is finally shown below. This was used to measure the voltage and current values on the battery after passing sinusoidal and PRBS perturbations. The reason for using for using a battery cell for applying DC current through the battery cell at test was to allow perturbations to be fed through the output load of the boost converter. The supply current from Battery cell 1 is fed into the boost converter through a circuit a breaker which was explained in section 4.3. The Mosfet driver and microcontroller are located on top of the converter. The NI-DAQ, PC with FFT conversion is connected to the far left. The microcontroller is also connected to the PC. The load in series with battery cell 1 is used to limit the current from the battery cell 2.



Figure 4.17: Experimental Set Up for EIS and PRBS Measurements

## Procedure of Experiment

The measurements are only taken when the converter voltage stabilises. To access when this point was reached, an oscilloscope was used to measure the output voltage across the output load of the boost converter. If the output voltage is within 10% of the  $V(c)$  voltage, then the system is stable.

Perturbations are then fed through the output load of the boost converter.

The PRBS was produced by the microcontroller as explained in chapter 4 earlier.

For EIS impedance measurements, the signal is fed using a function generator. The period for each perturbation was set to 20 seconds. As the experiment continues, the voltage across the capacitor will be measured as well by the oscilloscope. The process is halted if the value falls outside the boundary conditions which were described in section 3. The perturbation signals were fed during the charging and discharging of the converter. The figure below shows the simplified DC Boost converter system showing how it operates.

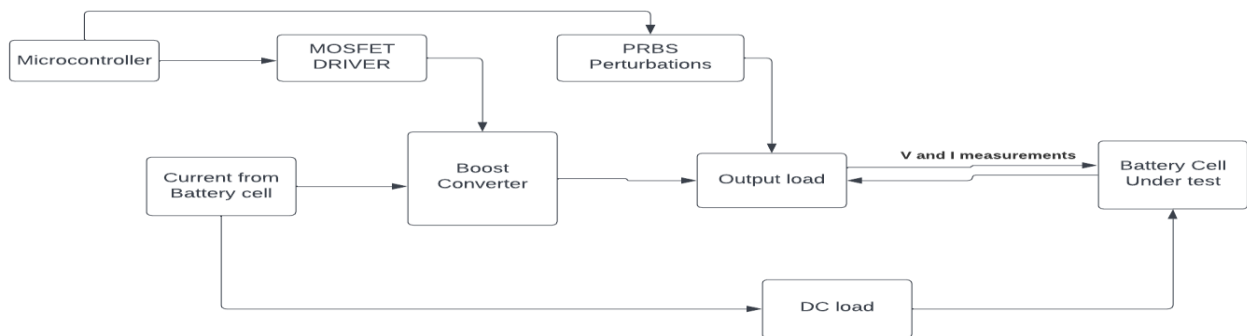


**Figure 4.18: Simplified model of the system**

Current and voltage variations across battery cell 2 are measured using voltage and current transducers, which are then input into a MATLAB function block. Both PRBS and EIS signal perturbations will have their BIS computed. In order to transform the measured values to frequency domain, an FFT is used to measure the signals using a ZOH, a buffer, a Hanning windowing function, and a ZOH. The following circuit was used in Simulink to determine impedance values in frequency domain.

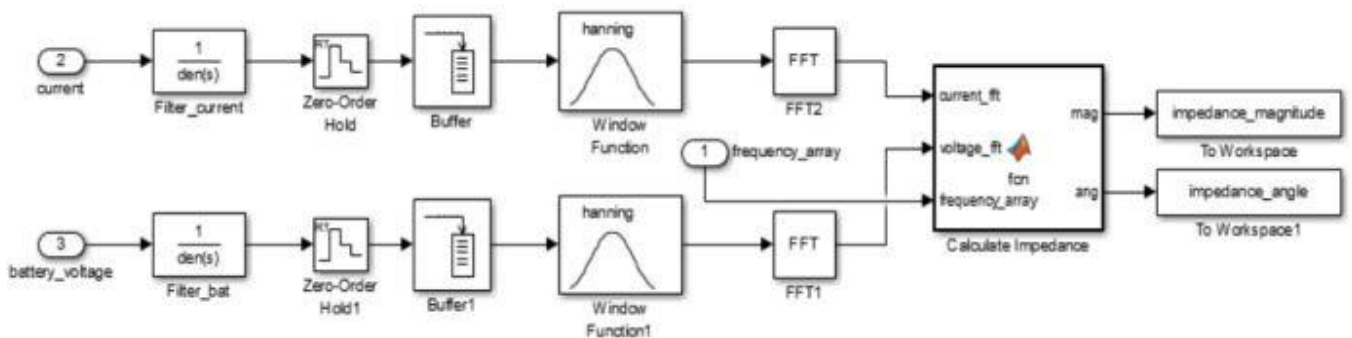


**Figure 4.19:FFT Operation**



## 5. Results

In this chapter, the switching boost converter EIS and PRBS test results are compared and analysed. Results from the bi-directional converter are acquired in both circumstances of charging and discharging.

### 5.1 Battery Impedance Measurements

The Li-Ion battery underwent the PRBS and EIS tests at room temperature with 100% SOC. A DC current of 0.75A would be needed for this. The basis of this test was to consider how well the electronic load performs.

#### 5.1.1 Plots During Discharge

The Li-Ion cell's Nyquist and Bode magnitude plot during discharge is shown in the Figure 5.1 below at 100% SOC. The impedance is pretty comparable to the impedance results from both 0.5A DC biases (reference). The Nyquist plots in Figure 5.2 below likewise showed little variation.

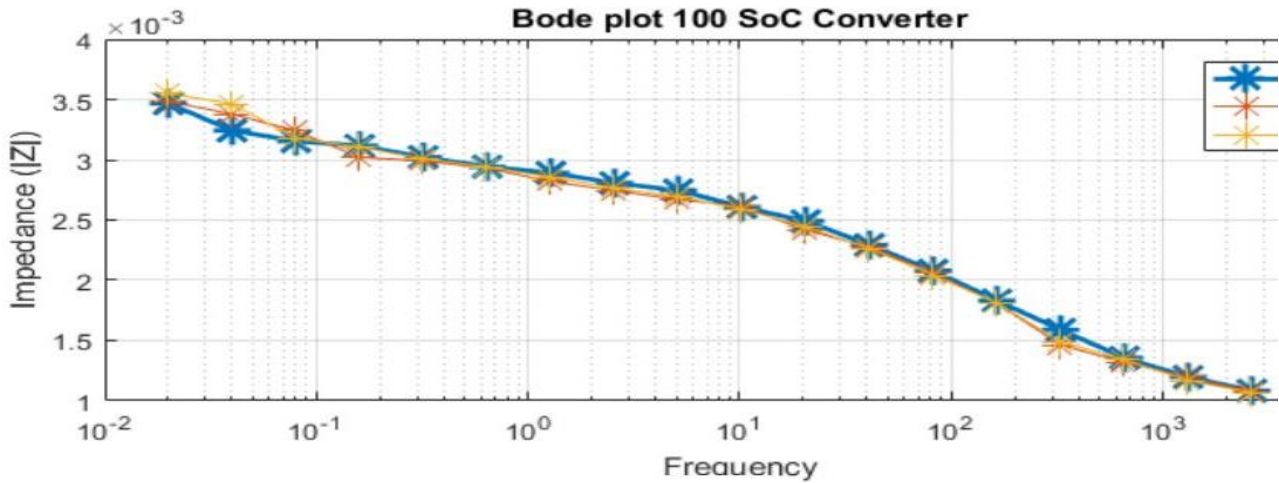


Figure 5.1: Results on a switching converter at 100% SOC whilst Discharging

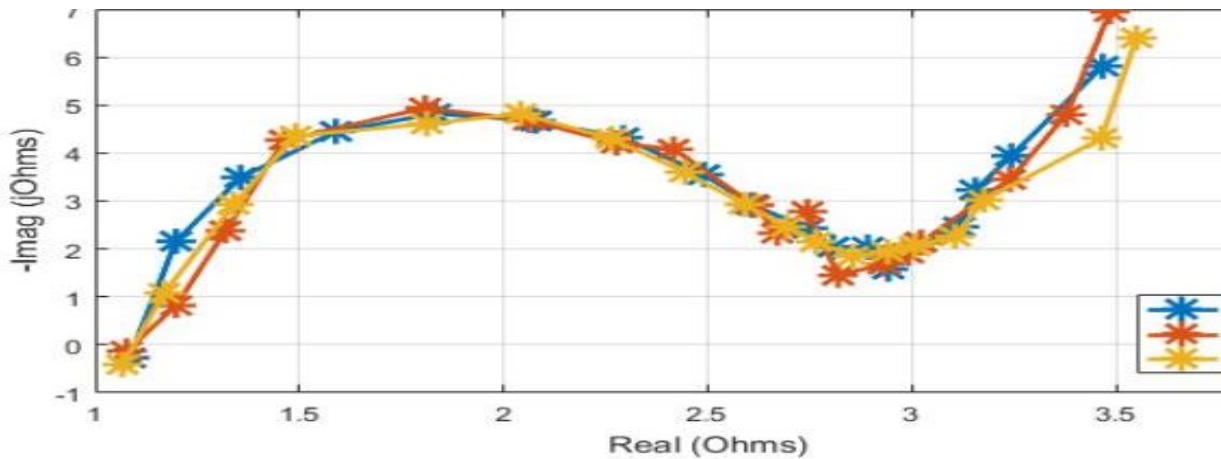


Figure 5.2: EIS(Yellow) and PRBS(Orange) at 100% SOC whilst Discharging

### 5.1.2 Plots During Charging

The Li-Ion battery was subsequently subjected to the same experiment at 100% SoC, however this time it was done for charging. This was done in order to demonstrate and evaluate the converter's capability to take EIS/PRBS measurements while it was charging. The effect of charging a Li-Ion cell at 100% SOC is shown in the figure below.

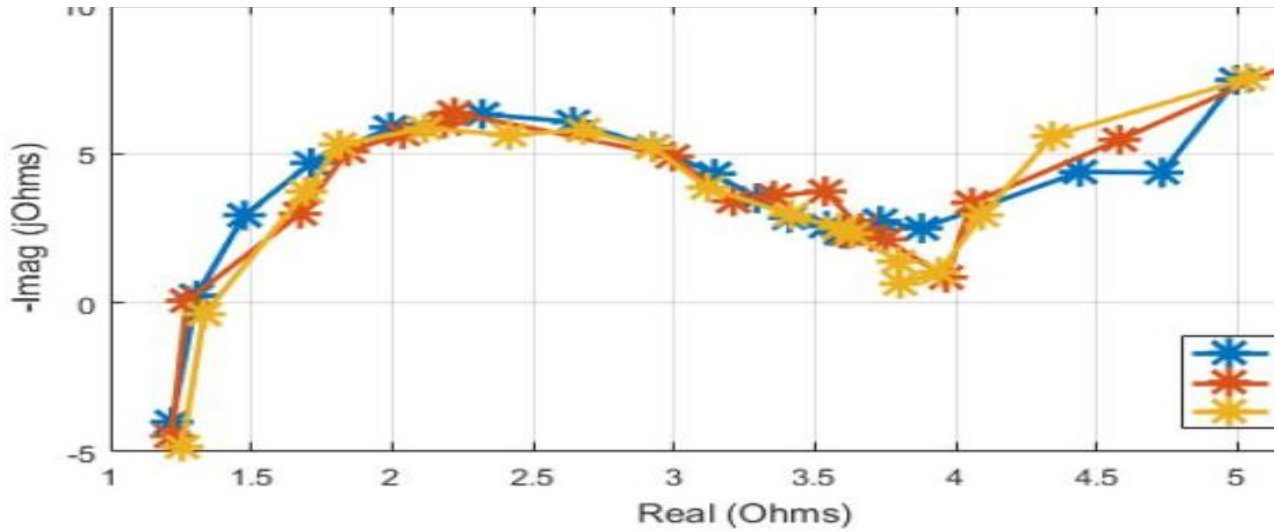


Figure 5.3: EIS(Yellow)and PRBS(Orange) at 100% SOC whilst Charging

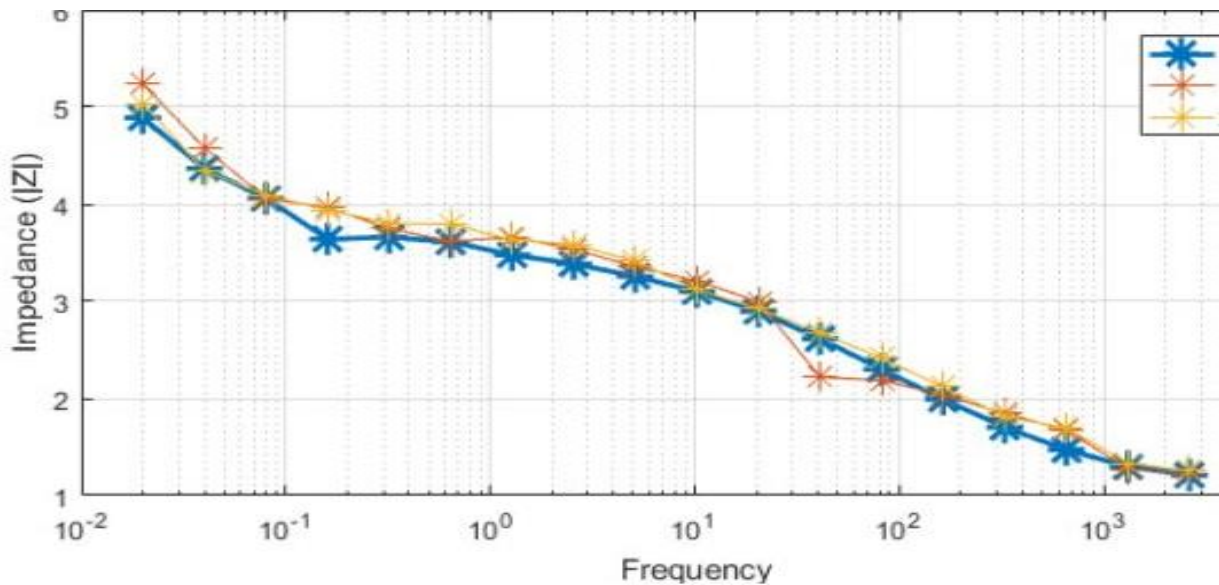


Figure 5.4: Results on a switching converter at 100% SOC whilst Charging

For upper and middle frequencies, the bode plot for the converter's EIS and PRBS correlates well with that of the reference, but strayed slightly for lower frequencies. The error analysis for each frequency's impedance was done, and the table below shows the average for each frequency group for 100 SOC. When the Li-Ion battery is at 100 SOC, the average inaccuracy is often less than 4% for the various frequency groups.

**Table 5.1: Boost Convertor Switching error for PRBS and EIS**

	Discharging		Charging	
Tests	EIS	PRBS	EIS	PRBS
frequency< 1	4.18	4.80	3.2	4.25
1< frequency<500	3.10	3.60	4.8	3.2
frequency>500	6.5	3.50	3.1	4.05
f ( All frequencies)	4.4	4.50	4.38	4.2

## 5.2 Noise In Output and Inductor Current

The high switching frequency component in the frequency spectrum produced by the 54kHz switching rate is another problem that needed to be addressed. The high switching frequency needed to be blocked by a low pass filter in order for the frequencies of the injected PRBS and EIS signal to pass through. All frequencies outside the cut-off frequency would be filtered out using ideal filters, while all other frequencies would be allowed to pass through the passband with no amplitude or phase changes.

The Figure below shows an image of the output current through the output load.

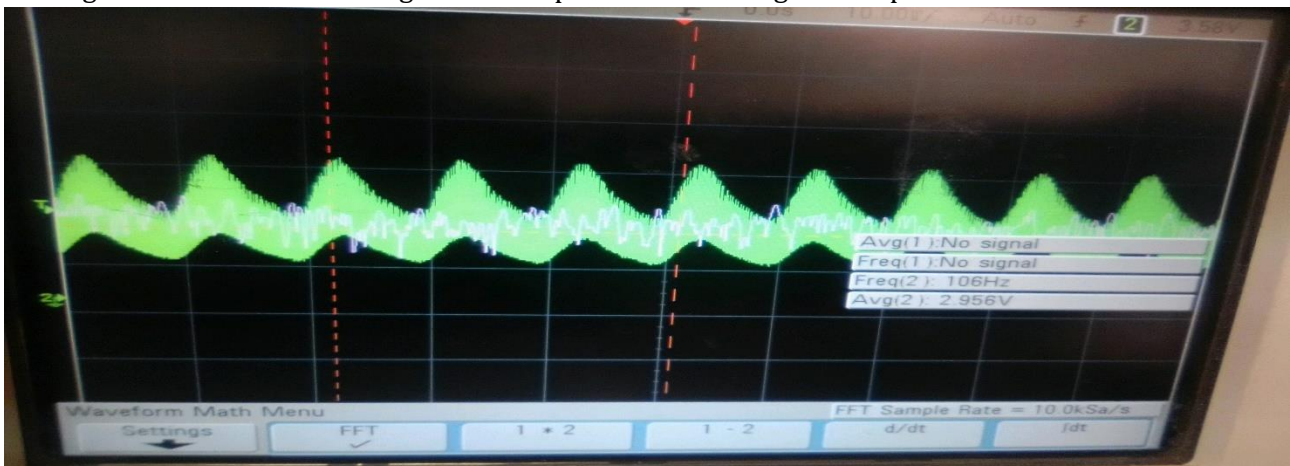


**Figure 5.5: Output Current through the load**

However, with time not permitting, the filter was not implemented. It is preferred that the detected perturbation's magnitude be as precise as practicable. Because of its flat bandpass, the Butterworth filter would need to be employed.

## 6. Discussion

---

The two methods used in this project demonstrate their ability to measure the battery's impedance with high accuracy, with the PRBS method having significantly lower errors for frequencies above 500 Hz. This might be because they interpret information differently (faster) than EIS. For lower frequencies, however, EIS deployment had resulted in better results. As a result, it becomes clear that PRBS is well suited for large-scale operations since it can tolerate extremely high frequencies with little inaccuracy. This would, however, need the use of extra power electronics in tandem with the power converter system in a realistic application. This might not be feasible depending on the size of the battery pack since a sizable heatsink might be required to disperse the heat produced by the converter.

It was determined that the EIS and PRBS performed by the DC-DC boost converter system was slightly less accurate than the prior technique according to literature review(reference). The IS signal, however, is being injected by the power converter itself and does not need any additional circuitry, making it more practical to deploy on any system.

The output inductor and output currents both had a lot of noise due to no filter being implemented.

The following were some of the practical difficulties encountered through the experimental work:

- a. Confirming that the length of the cables and connectors was adequate and that they did not add to the resistance that was determined from the battery.
- b. Maintaining the battery's temperature steadily during the measurements. A thermometer was used to keep an eye on this.
- c. Providing the battery with adequate downtime in between readings.
- d. Determining the correct parameters for the boost converter.

## 7. Conclusions

---

This project was set to investigate the practical implementation of Online Condition Monitoring of Lithium Batteries using Pseudo Random Binary Signals. Because they provide a lot of power for their size, lithium-ion batteries are widely used in electrical appliances and gadgets, and their ability to reconstruct in any shape or size due to the lightweight, compact design, and flexibility motivated this study.

The DC-DC bi-directional boost converter was used to test both EIS and PRBS. This was planned and put into action alongside a battery measurement system that could carry out both EIS and BIS. A cheap design of the system was used to execute it.

The results section noted that analogue Butterworth filters were particularly efficient in removing high frequency switching components from the test signals. Furthermore, it was demonstrated that EIS and PRBS on the dc/dc converter could be executed in both cases of charging or discharging of the battery.

For frequencies greater than 500 Hz, the PRBS technique exhibited much lower errors. This may be due to the fact that they analyse information more quickly and differently than EIS. EIS adoption, however, has produced better outcomes for lower frequencies. Thus, it is shown that PRBS is suitable for large-scale operations.

The use of a microcontroller or function generator to perform EIS and PRBS on a switching converter was then shown to be possible. The inductor current on the dc/dc converter can be accurately perturbed using small signal analysis. The battery voltage response was successfully produced by these changes in the inductor current, allowing for the analysis of resistance.



## 8. Recommendations

---

This section aims to provide recommendations for future research.

Future work must include the implementation of low pass filters so as to eliminate unwanted frequencies.

The Impedance Spectroscopy can be applied in different sectors around the and not just be limited to batteries.

Lowering the low frequency content of the AC Impedance signals to severely cut measurement time and identify the least number of impedance points necessary to give an accurate picture of the battery.

## 9. List of References

---

- [1] "Internal Resistance of Battery," *Physics Catalyst*, vol. 2, p. 1, 2019.
- [2] L. A. Middlemiss, "Characterisation of batteries by electrochemical impedance spectroscopy," *Energy Reports*, vol. 6, no. 4, pp. 232-241, 2020.
- [3] "Blue scientific," [Online]. Available: <https://blue-scientific.com/solartron-analytical/>. [Accessed 2022 September 16].
- [4] "Analog Devices," 2020. [Online]. Available: <https://www.analog.com/en/design-center/reference-designs/circuits-from-the-lab/cn0510.html#rd-overview>. [Accessed 3 September 2022].
- [5] "The electric Energy," 10 October 2013. [Online]. Available: <https://theelectricenergy.com/lithium-and-lithium-ion-battery/>. [Accessed 20 October 2022].
- [6] T. Stockley, "Advanced EIS Techniques for Performance," The International Federation of Automatic Control, Cape Town, South Africa, 2014.
- [7] I. H. Sardar, "A Short Review of Lithium-ion Battery Technology," *International Journal of Scientific Research in Science, Engineering and Technology*, vol. 7, no. 2, pp. v2394-4099, 2020.
- [8] "Agilent 33220A Function Generator," *UNIVERSITY OF CALIFORNIA AT BERKELEY*.
- [9] A. Andreas, "Using on-board Electrochemical Impedance Spectroscopy in," *EVS27*, vol. 6, p. 0793, 2013.
- [10] U. Westerhoff, "Analysis of Lithium-Ion Battery Models Based on Electrochemical Impedance Spectroscopy," *Wiley Online Library*, vol. 4, no. 12, pp. 1620-1630, 2016.
- [11] K. D.-I. Stroe, "Generalized Characterization Methodology for Performance Modelling of Lithium Batteries," *MDPI*, vol. 2, p. 37, 2016.
- [12] R. R. Thakkar, "Electrical Equivalent Circuit," Sardar Patel Institute of Technology, Mumbai, India, 2021.
- [13] A. Densmore, "Determining Battery SoC Using Electrochemical Impedance," IFEEC, Taipei, 2015.
- [14] M. Hannan, "A review of lithium-ion battery state of charge estimation and recommendations".
- [15] T. Stockley, "Advanced EIS Techniques for performance," IFAC World Congress, Cape Town, 2014.
- [16] B. Paul and W. A, "A comparison of the different broadband impedance measurement," 2016 IEEE Energy Conversion Congress and Exposition, Milwaukee, 2016.
- [17] R. Koch, "Impedance Spectroscopy for Battery Monitoring with Switched," IEE, Pitsburg, 2014.
- [18] P. Barendse and O. Alao, "Online Condition Monitoring of Sealed Lead Acid & Lithium Nickel-Cobalt-Manganese Oxide Batteries using Broadband Impedance Spectroscopy," IEEE, Portland, OR, USA, 2018.
- [19] Gamry, "Basics of Electrochemical Impedance Spectroscopy," 18 September 2017. [Online]. Available: <https://www.gamry.com/application-notes/EIS/basics-of-electrochemical-impedance-spectroscopy/>. [Accessed 6 October 2022].
- [20] J. Sihvo, "Fast Approach for Battery Impedance Identification Using Pseudo-Random Sequence Signals," *IEEE TRANSACTIONS ON POWER ELECTRONICS*, vol. 35, no. 3, pp. 2548-2557, 2020.
- [21] S. Mhlangu, "Online monitoring of Lithium-ion batteries using Broadband Signal," Bachelors of Science Dissertation, Dept. Elect. Eng., University of Cape Town, Cape Town, WC, 2019.
- [22] V. J. Ovegas, "Impedance Characterization of an LCO-NMC/Graphite Cell: Ohmic Conduction, SEI Transport and Charge-Transfer Phenomenon," *batteries*, vol. 4, no. 3, p. 43, 2018.
- [23] J. D. Kramer and C. Jacky, "How to write biblos," vol. 1, no. 1, 2006.
- [24] S.-R. Chou, "Fast Estimation of State of Charge for Lithium-Ion Batteries," *energies*, vol. 7, pp. 3438-3452, 2014.
- [25] S. Moore and P. Barendse, "Online condition monitoring of lithium-ion batteries using impedance

spectroscopy," IEEE, Cincinnati, OH, USA, 2017.

- [26] M. Urquidi-Macdonald, "Applications of Kramers—Kronig transforms in the analysis of electrochemical impedance data—III. Stability and linearity," *Electrochimica Acta*, vol. 35, no. 10, pp. 1559-1566, 1990.
- [27] J. J. Sihvo, T. Messo, T. Roinila and R. Luht, "Online Internal Impedance Measurements of Li-ion Battery Using PRBS Broadband Excitation and Fourier Techniques: Methods and Injection Design," IEEE, Niigata, Japan, 2018.
- [28] B. Chapman, "How does a lithium-Ion battery work?," 23 September 2019. [Online]. Available: <https://letstalkscience.ca/educational-resources/stem-in-context/how-does-a-lithium-ion-battery-work#:~:text=When%20the%20battery%20is%20charging,to%20keep%20your%20device%20running..> [Accessed 7 September 2022].
- [29] S. L. Li and X. P. Ai, "A polytriphenylamine-modified separator with reversible," *Journal of Power Sources*, vol. 189, no. 1, p. 771–774, 2009.
- [30] J. K. Feng, X. P. Ai and Y. L. Cao, "Polytriphenylamine used as an electroactive separator," *Journal of Power Sources*, vol. 161, no. 1, p. 545–549, 2016.
- [31] U. Westerhoff, "Analysis of Lithium-Ion Battery," *Energy Technology*, vol. 4, p. 1620–1630, 2016.
- [32] E. Barsoukov, "Impedance Spectroscopy Theory, Experiment, and Applications, New Jersey: John Wiley and Sons, Inc, 2005.
- [33] X. Wang and X. Wei, "Estimation of state of health of lithium-ion batteries based on," *Journal of Energy Storage*, vol. 21, pp. 618-631, 2019.
- [34] Y. Abe, N. Hori and S. Kumagai, "Electrochemical Impedance Spectroscopy on the Performance Degradation of LiFePO<sub>4</sub>/Graphite Lithium-Ion Battery Due to Charge-Discharge Cycling under Different C-Rates," *Energies*, vol. 12, 2019.
- [35] A. Wang, "Review on modeling of the anode solid electrolyte interphase (SEI) for lithium-ion batteries," *Computational Materials*, vol. 4, no. 1, 2018.
- [36] N. A. Chaturvedi, "Algorithms for Advanced Battery-Management Systems," IEEE, 2010.



### B.3

#### EIS Generation in Simulink

```
%ind = [50.5 115 200 615];
for ind = [50.5 115 200 615]
    seriInd = (1E-9)*ind;
    % EIS full sine sweep simulation and data collection
    % Instantiate variables
    samps = 24;
    freq_n = 0;
    zMag = [];
    zAngle = [];
    totalTime = 0;
    % Iterate over sine sweep frequencies
    for n = 1:24
        freq_n = 1.5^(n);
        mdlWks = get_param('EIS_Simulation_V2_R2022b', 'ModelWorkspace');
        assignin(mdlWks, 'injectFreq', freq_n);
        eisSim = sim('EIS_Simulation_V2_R2022b', ((n+2)*2*pi)/(freq_n));

        % Collect impedance results in polar form
        newZmag = eisSim.absZ;
        newZangle = eisSim.phiZ;
        totalTime = totalTime + ((n+2)*2*pi)/(freq_n);
```

#### Analysis of Obtained EIS Results

```
% Impedance
newZmag = eisSim.absZ;
newZangle = eisSim.phiZ;
totalTime = totalTime + ((n+2)*2*pi)/(freq_n);
% Assimilate full sweep results. Average and isolate useful data
zMag = [zMag; mean(newZmag((floor(3*length(newZmag)/4)):end))];
zAngle = [zAngle; mean(newZangle((floor(3*length(newZangle)/4)):end))];
end
% Convert to rectangular form
zImag = zMag.*sind(zAngle);
zReal = zMag.*cosd(zAngle);

% Plot Nyquist diagram
plot(zReal, -zImag)
xlabel("RealZ")
ylabel("- ImagZ")
title("Theoretical and real combined")
hold on
```

### B.3

#### Theoretical Simulation in Simulink Using R, L and C values

```
%Theoretical Code
R1 = 0.001;
R2 = 0.0002;
R3 = 0.0015;
R4 = 0.003;
C1 = 2;
C2 = 15;
C3 = 500;
L = 40*(10^-9);
w = 1:0.1:16384;
Z = R1 + 1i.*w.*L + 1./(1i.*w.*C1 + 1/R2) +
1./(1i.*w.*C2 + 1/R3) + 1./(1i.*w.*C3 + 1/R4);
plot(real(Z), -imag(Z))
xlim([0.00083 0.00900])
ylim ([-0.00083 0.00197])
xlabel("RealZ")
ylabel("- ImagZ")
title("Theoretical Complex Impedence Model")

hold off
end
```



# 11. EBE Faculty: Assessment of Ethics in Research Projects

Application for Approval of Ethics in Research (EIR) Projects Faculty of Engineering and the Built Environment, University of Cape Town

## ETHICS APPLICATION FORM

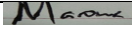

Please Note:

Any person planning to undertake research in the Faculty of Engineering and the Built Environment (EBE) at the University of Cape Town is required to complete this form **before** collecting or analyzing data. The objective of submitting this application *prior* to embarking on research is to ensure that the highest ethical standards in research, conducted under the auspices of the EBE Faculty, are met. Please ensure that you have read, and understood the **EBE Ethics in Research Handbook** (available from the UCT EBE, Research Ethics website) prior to completing this application form: <http://www.ebe.uct.ac.za/ebe/research/ethics1>

APPLICANT'S DETAILS		
Name of principal researcher, student, or external applicant		Nigel Marowa
Department		EBE
Preferred email address of applicant:		MRWNIG002@myuct.ac.za
If Student	Your Degree: e.g., MSc, PhD, etc.	BSc in Mechatronics Engineering
	Credit Value of Research: e.g., 60/120/180/360 etc.	40
	Name of Supervisor (if supervised):	Professor Barendse, Paul
If this is a research contract, indicate the source of funding/sponsorship		N/A
Project Title		Practical implementation of Online Condition Monitoring of Lithium-Ion Batteries using Pseudo Random Signals.

**I hereby undertake to carry out my research in such a way that:**

- there is no apparent legal objection to the nature or the method of research; and
- the research will not compromise staff or students or the other responsibilities of the University;
- the stated objective will be achieved, and the findings will have a high degree of validity;
- limitations and alternative interpretations will be considered;
- the findings could be subject to peer review and publicly available; and
- I will comply with the conventions of copyright and avoid any practice that would constitute plagiarism.

APPLICATION BY	Full name	Signature	Date
<b>Principal Researcher/ Student/External applicant</b>	Nigel Marowa		18/08/22
SUPPORTED BY	Full name	Signature	Date
<b>Supervisor (where applicable)</b>	Professor Barendse, Paul		18/08/2022
APPROVED BY	Full name	Signature	Date
<b>HOD (or delegated nominee)</b> Final authority for all applicants who have answered NO to all questions in Section 1; and for all Undergraduate research (Including Honors).			

<b>Chair: Faculty EIR Committee</b> For applicants other than undergraduate students who have answered YES to any of the questions in Section 1.			
---	--	--	--



**ADDENDUM 1:**

<b>Student proposed?</b>	Y/N	N
<b>ID:</b>	<b>PB02</b>	
<b>SUPERVISOR:</b>	<b>BARENDSE</b>	
<b>TITLE:</b>	<b>Practical implementation of Online Condition Monitoring of Lithium Ion Batteries using Pseudo Random Signals.</b>	
<b>DESCRIPTION:</b>	<p>Most new battery research has focused on the development of new materials in the pursuit of higher energy and power density, longer cycle-life and shorter recharge times. However, successfully predicting and managing the life of batteries is in equal parts necessary for widespread adoption of these cutting edge technologies. Lithium ion batteries have a high power to weight ratio making it popular in electrical equipment and devices. Due to the compact size, weight and flexibility of remodelling in any shape and size, it is widely used in electric vehicles. In this case lithium-ion battery is used for EV's, power consumption varies therefore it is critical to be monitor the performance and state of health, while also implementing optimal energy management strategies. The purpose of the project is to design an online monitoring system for a battery performance, specifically using <b><u>pseudorandom signals</u></b> for attaining <b><u>impedance information</u></b>. Time permitting, a ternary sequence with better tolerance to battery nonlinear effects, with comprehensive amplitude and filtering design for battery impedance measurements will also be considered</p>	

[1] . Please see figure below for an example of a battery monitoring system. This is a continuation of a project from 2020, whereby the system was simulated. This project will focus on the implementation of the system.

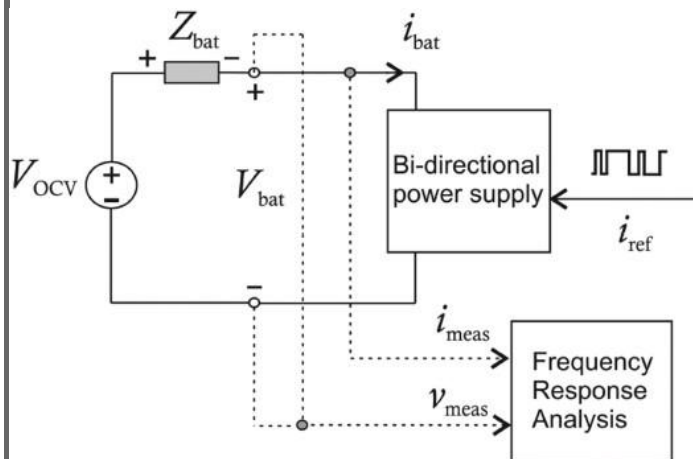


Figure 4: Implementation of the pseudo-random binary sequence scheme

Reference:

[1] J. Sihvo, D. Stroe, T. Messo and T. Roinila, "Fast Approach for Battery Impedance Identification Using Pseudo-Random Sequence Signals," in *IEEE Transactions on Power Electronics*, vol. 35, no. 3, pp. 2548-2557, March 2020.

#### DELIVERABLES:

The main objectives of the project is to:  
 conduct a literature review on lithium ion batteries, modelling techniques, performance and state of health assessment  
 develop an electrical equivalent circuit model of the battery  
 design and develop a converter for injecting pseudo random signals into the battery , using an electronic load  
 Analyse the results and discuss findings  
 Draw conclusions and make recommendations

#### SKILLS/REQUIREMENTS:

Power electronics, control, analytical and mathematical skills.

Software required: Matlab Simulink

**GA 1: Problem solving:**  
*Identify, formulate, analyse and solve complex\* engineering problems creatively and innovatively*

Design of a condition monitoring technique for batteries using pseudorandom signals to extract impedance information.

**GA 4\*\*:** **Investigations, experiments and analysis:** *Demonstrate competence to design and conduct investigations and experiments.*

Once the system has been designed and simulated, conduct investigations to evaluate the effectiveness of using pseudorandom signals for extracting impedance information.

#### EXTRA INFORMATION:

For further information please e-mail me at [paul.barendse@uct.ac.za](mailto:paul.barendse@uct.ac.za).

<b>BROAD Research Area:</b>	Energy Engineering (Power Electronics and Control)
<b>ETHICS</b>	No
<b>Project suitable for ME/ ECE/EE/ALL?</b>	ME/EE

**ADDENDUM 2:** To be completed if you answered YES to Question 2:

It is assumed that you have read the UCT Code for Research involving Human Subjects (available at <http://web.uct.ac.za/depts/educate/download/uctcodeforresearchinvolvinghumansubjects.pdf>) in order to be able to answer the questions in this addendum.

2.1 Does the research discriminate against participation by individuals, or differentiate between participants, on the grounds of gender, race or ethnic group, age range, religion, income, handicap, illness or any similar classification?	YES	NO
2.2 Does the research require the participation of Socially or physically vulnerable people (children, aged, disabled, etc) or legally restricted groups?	YES	NO
2.3 Will you not be able to secure the informed consent of all participants in the research? (In the case of children, will you not be able to obtain the consent of their guardians or parents?)	YES	NO
2.4 Will any confidential data be collected or will identifiable records of individuals be kept?	YES	NO
2.5 In reporting on this research is there any possibility that you will not be able to keep the identities of the individuals involved anonymous?	YES	NO
2.6 Are there any foreseeable risks of physical, psychological or SOcial harm to participants that might occur in the course of the research?	YES	NO
2.7 Does the research include making payments or giving gifts to any participants?	YES	NO

If you have answered YES to any of these questions, please describe below how you plan to address these issues:

**ADDENDUM 3:** To be completed if you answered YES to Question 3:

3.1 Is the community expected to make decisions for, during or based on the research?	YES	NO
3.2 At the end of the research will any economic or SOCial process be terminated or left unsupported, or equipment or facilities used in the research be recovered from the participants or community?	YES	NO
3.3 Will any service be provided at a level below the generally accepted standards?	YES	NO

If you have answered YES to any of these questions, please describe below how you plan to address these issues:

**ADDENDUM 4:** To be completed if you answered YES to Question 4

4.1 Is there any existing or potential conflict of interest between a research sponsor, academic supervisor, other researchers or participants?	YES	NO
4.2 Will information that reveals the identity of participants be supplied to a research sponsor, other than with the permission of the individuals?	YES	NO
4.3 Does the proposed research potentially conflict with the research of any other individual or group within the University?	YES	NO

If you have answered YES to any of these questions, please describe below how you plan to address these issues: